

DeepTransition: Viability Leads to the Emergence of Gait Transitions in Learning Anticipatory Quadrupedal Locomotion Skills

Milad Shafiee¹, Guillaume Bellegarda¹, and Auke Ijspeert¹

¹Biorobotics Laboratory, École Polytechnique Fédérale de Lausanne (EPFL), 1015 Lausanne, Switzerland

ABSTRACT

Quadruped animals seamlessly transition between gaits as they change locomotion speeds. While the most widely accepted explanation for gait transitions is energy efficiency, there is no clear consensus on the determining factor, nor on the potential effects from terrain properties. In this article, we propose that viability, i.e. the avoidance of falls, represents an important criterion for gait transitions. We investigate the emergence of gait transitions through the interaction between supraspinal drive (brain), the central pattern generator in the spinal cord, the body, and exteroceptive sensing by leveraging deep reinforcement learning and robotics tools. Consistent with quadruped animal data, we show that the walk-trot gait transition for quadruped robots on flat terrain improves both viability and energy efficiency. Furthermore, we investigate the effects of discrete terrain (i.e. crossing successive gaps) on imposing gait transitions, and find the emergence of trot-pronk transitions to avoid non-viable states. Compared with other potential criteria such as peak forces and energy efficiency, viability is the only improved factor after gait transitions on both flat and discrete gap terrains, suggesting that viability could be a primary and universal objective of gait transitions, while other criteria are secondary objectives and/or a consequence of viability. Moreover, we deploy our learned controller in sim-to-real hardware experiments and demonstrate state-of-the-art quadruped agility in challenging scenarios, where the Unitree A1 quadruped autonomously transitions gaits between trot and pronk to cross consecutive gaps of up to 30 cm (83.3% of the body-length) at over 1.3 m/s.

Introduction

Quadruped animals learn impressive abilities to traverse challenging terrain, reach remote parts of the planet, and perform agile locomotion in pursuit of prey. They learn to avoid falling in all of these locomotion scenarios, which in robotics terms means staying *viable*. Such fascinating locomotion skills emerge from inter-limb coordination governed by the interaction between the brain, the spinal cord, and the musculoskeletal system¹. The modulation of this inter-limb coordination can produce different gait patterns, and the transition between these patterns is a fundamental feature of locomotion. Quadruped animals smoothly transition between different locomotion gaits such as walking, trotting, galloping, and bounding/pronking depending on their speed. However, despite the growing number of studies on gait transitions in both robotics and biology, there is still no clear consensus regarding the underlying mechanisms as well as the criteria that determine why gait transitions take place in different conditions.

Different quantities have been proposed as important in gait transitions: energy expenditure, peak forces, and periodicity. A study conducted by Hoyt and Taylor² suggested that, when changing locomotion speed, horses switch gaits to reduce energy expenditure. While energy efficiency is now the most widely accepted objective for gait transitions, other studies have found that this hypothesis may not always be valid for humans³⁻⁵. As an alternative to the energy-efficiency hypothesis, Farley and Taylor⁶ have suggested that the trot-gallop gait transition in horses is triggered when peak musculoskeletal forces reach a critical level. In particular, transitioning between gaits makes it possible to reduce peak musculoskeletal forces (and consequently the risk of injury). However, at the transition speed, galloping requires more energy than trotting, meaning that this gait transition increases the Cost of Transport (CoT). Therefore, the second suggested criterion for gait transitions is reducing peak musculoskeletal forces. Granatosky et al.⁷ observe that, across nine species, gait periodicity (computed by measuring inter-stride variability) predicts the occurrence of gait transitions better than energy efficiency. Their findings suggest that gait transitions are performed such as to maximize periodicity (i.e. minimize inter-stride variability) and avoid unstable gaits. They link periodicity to stability, and hypothesize that periodicity (and hence stability) is another important gait transition criteria on flat terrain. High periodicity can furthermore be useful for anticipatory behavior on flat terrain by simplifying the prediction of future states (e.g. future foot placements). However, periodicity is not necessarily a good feature *per se*, in particular when the terrain is irregular.

Animal experiments have played a crucial role in exploring the criteria for gait transitions in the aforementioned research. In

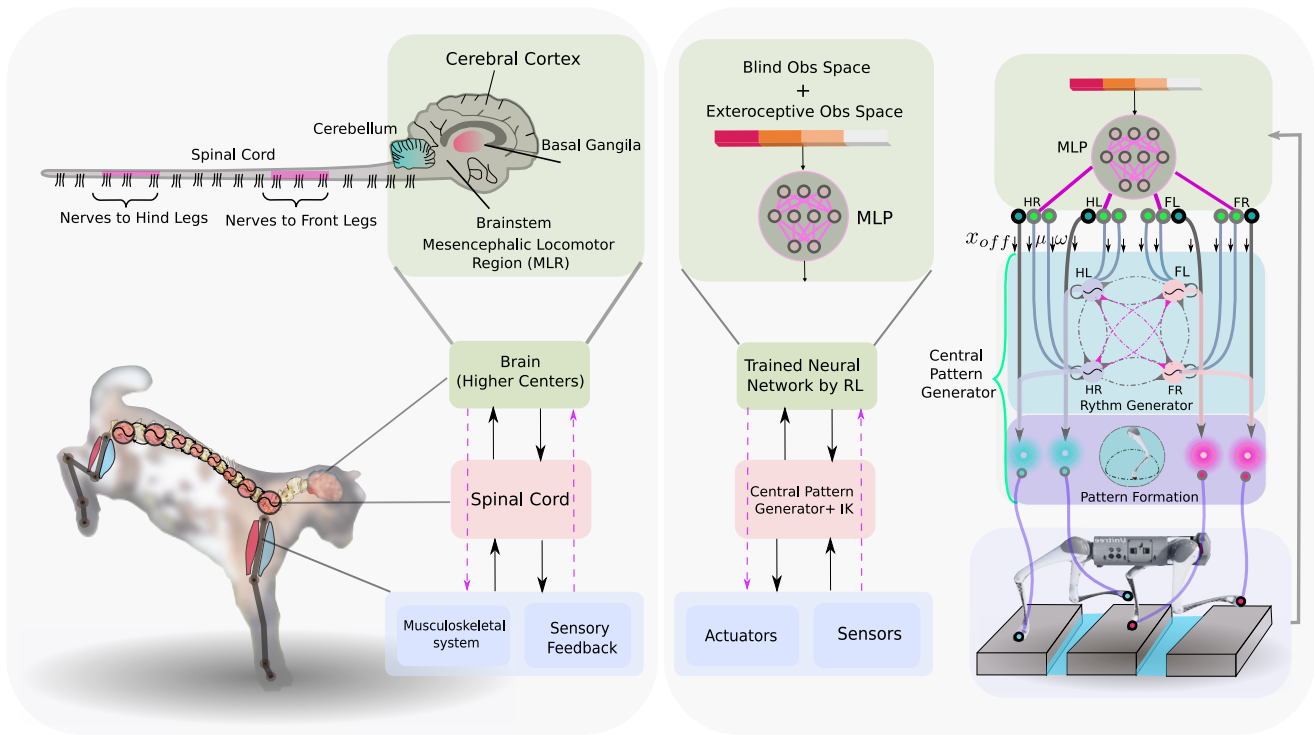


Figure 1. To model locomotion control, we consider three main interacting layers: the brain (higher centers), the spinal cord, and the body and sensory feedback modules. Higher neural centers (such as the brainstem, basal ganglia, cerebellum, and motor cortex) send descending drive signals to modulate the spinal circuits, and/or directly interact with lower modules (body and sensory feedback). We represent these higher neural centers with a multilayer perceptron with three hidden layers of [512, 256, 128] neurons with `relu` activation. To represent the Central Pattern Generator in the spinal cord, we use nonlinear amplitude-controlled phase oscillators for modeling the Rhythm Generator (RG) layer, whose outputs are mapped to foot positions and then motor commands with inverse kinematics (IK) through a Pattern Formation (PF) layer. The left brain figure has been re-drawn with inspiration from Grillner et. al.¹ (CC BY 4.0).

particular, experiments with spinal transections and decerebrations in cats have been instrumental in establishing the functional roles of the neural circuits in the spinal cord during locomotion^{8,9}. For example, physiological studies have found that electrical stimulation or increasing the speed of a motorized treadmill can cause a decerebrated cat to spontaneously change gaits^{10–12}. However, such animal experiments clearly raise ethical issues, making extensive data collection impossible. As an alternative, we can use robots as tools to investigate scientific hypotheses about animal motor-control, iteratively taking inspiration from animals to improve the robots' performance^{13–18}. Robots allow us to test computational models of the spinal cord in closed-loop to measure internal states during agile locomotion on challenging terrains, which is not possible with animals.

In robotics, abstract models of the spinal cord composed of central pattern generators (CPGs), i.e. systems of coupled oscillators, and reflexes are commonly used for locomotion pattern generation^{19–24} as well as for the investigation of biological hypotheses^{25,26}. CPGs provide an intuitive formulation for specifying different gaits²⁷, and spontaneous gait transitions can arise by increasing descending drive signals and incorporating contact force feedback^{28,29} or vestibular feedback³⁰. Within a dynamical systems context, it has been suggested that gait transitions serve to avoid unstable states^{31–34}. Gaits can be viewed as a result of complex systems that self-organize around their natural dynamics, and gait transitions occur when the stability of the system dynamics decreases so much that switching to a new gait increases stability. With this dynamical systems analysis, the CoT is described as a surrogate for the stability of the underlying dynamics, but it is not considered as a primary determinant *per se*, since gaits with lower stability necessitate active control for stabilization, which consequently results in higher energy consumption. Recent studies have shown the possibility of acquiring different gaits through deep reinforcement learning (DRL)^{35–42}. While gait transitions did not autonomously emerge within these learning frameworks, the walk-trot transitions were found possible through a combination of model predictive control (MPC) and DRL by minimizing energy consumption⁴³.

In summary, animal and robotics investigations suggest so far that energy efficiency, stability, and avoiding peak forces (injury) to the musculoskeletal system are plausible explanations for animals to transition between different gaits. In this article, we explore the potential role of another criterion: the concept of *viability*, which formalizes the notion of avoiding a fall during

legged locomotion. Viable states are all of the states starting from which a system can avoid falling through proper action selection^{44,45}. Viability is a useful general objective for locomotion control, and it is influenced by multiple factors such as periodicity, gait stability (in a Lyapunov sense), and negative events such as falls into a gap or collisions with obstacles. While viability is related to periodicity and gait stability, it is a broader concept. For example, higher periodicity might in general increase viability on flat terrain as it tends to reduce the number of falls, but not so on irregular terrains which require discrete step-to-step adjustments. Such considerations make viability more difficult to explicitly measure. In this article, we use the general concept *viability* to describe gait stability and periodicity during locomotion on flat terrain, as well as fall avoidance during gap-crossing scenarios.

We use a hierarchical biology-inspired framework leveraging robotics and DRL tools⁴⁶ to investigate the following research questions surrounding the emergence of quadruped gait transitions:

1. What are the plausible determinants for quadruped animal gait transitions from the following options: minimization of Cost of Transport (CoT), minimization of peak forces, and/or viability?
2. Given that animals such as horses use certain gaits at specified velocity ranges, what is the explanation for the shallower CoT-Velocity plot of “normal” walk/trot gaits, compared with extended walk/trot gaits (i.e. when using a gait outside of nominally trained operating regions)?
3. Does the environment (i.e. a terrain with gaps) impose certain gaits, and how does anticipatory sensing of upcoming terrain affect gait transitions? What is the relationship between gait transitions imposed by the terrain, and the aforementioned criteria of CoT, peak contact forces, and viability?
4. What kind of exteroceptive sensory information is most effective (and sufficient) for triggering gait transitions when a legged system must cross a terrain with gaps?

To answer these questions, we investigate the interaction between supraspinal drive and a CPG to produce anticipatory locomotion for a quadruped robot⁴⁶. Using DRL, we train a neural network policy to replicate the supraspinal drive behavior. This policy can either modulate the CPG dynamics, or directly change actuation signals to bypass the CPG dynamics. We design two experimental setups for investigating locomotion on either flat terrain, or on terrains with variable gaps.

On flat terrain, we investigate the first two research questions by examining the consistency of the proposed abstract motor-control architecture with two different sets of quadruped animal data^{2,7}. With the first set of data from Granatosky et al.⁷, we compare the quadruped robot CoT and periodicity for walking and trotting gaits under “normal” conditions with data from domestic dogs (*Canis lupus familiaris*), Australian water rats (*Hydromys chrysogaster*), Virginia opossums (*Didelphis virginiana*), and tufted capuchins (*Sapajus apella*). The results suggest that there is an optimal velocity for walk-trot gait transitions which reduces energy expenditure and improves periodicity (which we see as an indicator for viability on flat terrain, see Methods). These results conjecture that energy efficiency and periodicity (viability) are inter-related for explaining gait transitions. The second set of data from Hoyt and Taylor² shows extended gaits for horses, where the horses have learned to walk and trot outside of their “normal” gait operating regimes. We compare extending walking and trotting gaits for our quadruped robot to locomote outside of the velocity ranges for which it has trained for, and show comparable CoT curves with those of the horses. The curvature is much greater for the extended gaits, as the locomotion policies have not been optimized for these velocity regions for the specified gaits in both animals and robots, as both systems encounter new sets of parameters/observations.

On variable gap terrains, to the best of our knowledge, we investigate for the first time the role of environmental perception and anticipation in the context of quadrupedal gait transitions. Focusing on questions three and four, our results suggest that viability is the dominant criteria for gait transitions in anticipatory scenarios. Moreover, our results show that foot distance to a gap, and in particular the front foot distance, is the most important visually-extracted exteroceptive sensory information for successful gap crossing, and that vestibular information plays a key role in the emergence and transition to the pronk gait.

Finally, we demonstrate that our hierarchical biology-inspired control architecture enables the Unitree A1 quadruped robot to cross challenging gap terrains of up to 30 cm in width (83.3% of the body-length) in sim-to-real hardware experiments. To the best of our knowledge, this represents the most dynamic crossing of such large consecutive gaps for a quadrupedal robot, where A1 exhibits a trot-pronk gait transition to locomote at over 4.68 km/h (1.3 m/s). Moreover, this is the first learning-based locomotion framework in which gait transitions emerge spontaneously during the learning process without having a dynamical model, MPC, curriculum, or mentor in the loop.

Results

In this section, we investigate and present locomotion results in two environmental scenarios: one for flat terrain and another for discrete gap terrain. In the discrete gap terrain, we investigate the objective for gait transitions by considering three main

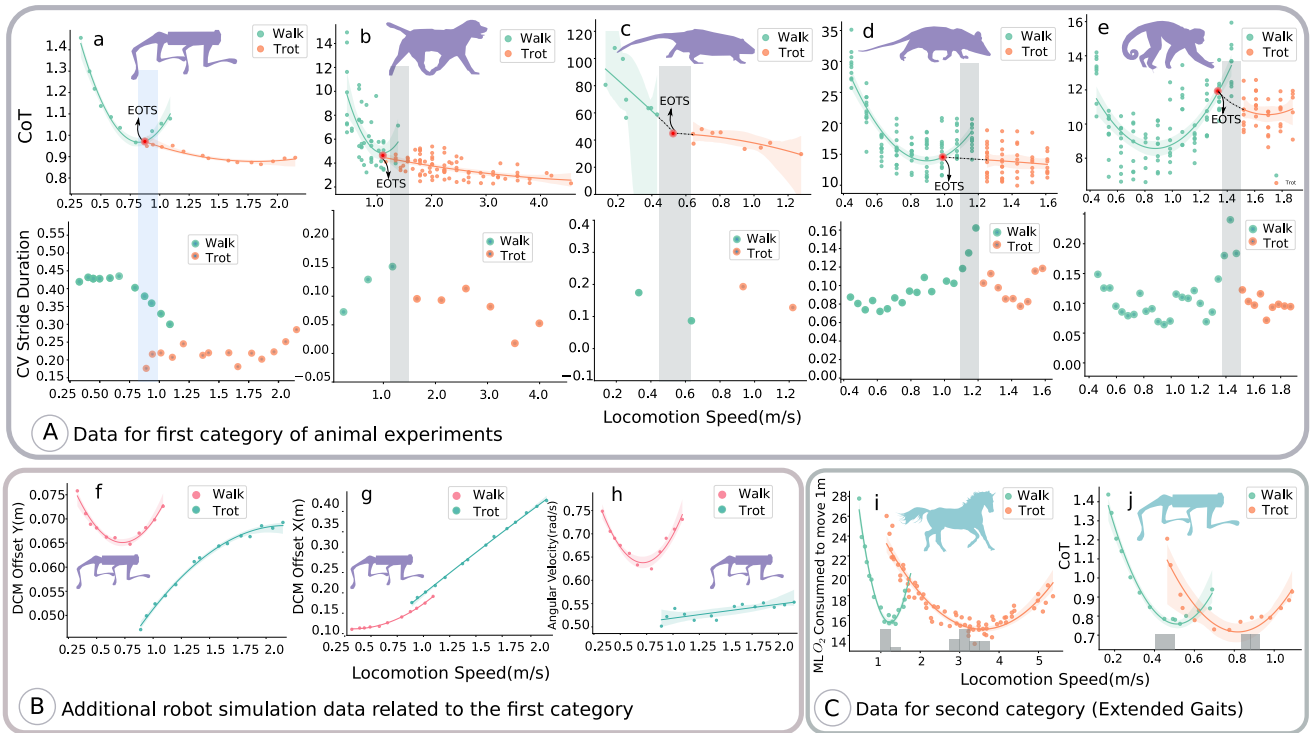


Figure 2. Qualitative comparison data for robot and animal locomotion. **A:** The CoT and CV of stride duration of the animals and the robot are plotted against the locomotion speed of walk-trot gaits in: a) the quadruped robot, b) the domestic dog, c) the Australian water rat, d) the Virginia opossum and e) the tufted capuchin. This data relates to the first category of animal experiments with normal gaits from Granatosky et al.⁷. The shadow vertical bars in (b)-(e) represent the range of preferred gait transition speeds for animals. In (a), the blue bar indicates the expected transition speed for the robot. The speed at which the CoT curve for a walking gait intersects with the CoT curve for a trotting gait represents the energetically optimal transition speed (EOTS). **B:** The DCM offset and average body angular velocity from the robot simulation in (a). **C:** The CoT is plotted against locomotion speed for the second category of animal data, i.e. horses with extended gaits from Hoyt and Taylor². The shadow bar in (i) represents the speed at which horses prefer to locomote for that particular gait. In a lifelong learning process, this is the velocity for which the horse’s motor control has been optimized for each gait². In (j), the gray shadow bar represents the speed at which the policy is trained. The shaded area around the interpolated curves indicates the 95% confidence interval of interpolation. For the CV of stride duration for the animal data, Granatosky et al.⁷ have calculated the mean of the stride duration for the specific speed interval. We report average values for testing the policies for 35000 sample (7 tests of 5 s of locomotion) since the standard deviations are small (i.e. less than 10% of the mean), and the standard deviations are reported in the supplementary material.

elements in the reward function: viability, CoT, and peak contact forces. When training the locomotion policies, we consider the effects of three different values (high, medium, and low) for the reward weights. Our analysis of these reward function term weights reveals that the combination of high, low, and low weights for viability, CoT, and peak forces, respectively, yields the best performance (highest gap crossing success rate).

On flat terrain, we train distinct policies for our robot to learn locomotion at various velocities, focusing on specific gaits such as walk and trot. To achieve different velocities, we incorporate a velocity tracking term into the reward function. On flat terrain, each gait is achieved by utilizing explicit oscillator phase coupling matrices in the abstract CPG equations, specifically defined for walk and trot (see Methods and Supplementary Material). In this scenario, along with the velocity tracking term, our reward function gives a high weight to viability and a low weight to energy consumption, similar to the best gap crossing scenario result. We do not include the peak force component in the reward function for blind locomotion, as our investigation on flat terrain is centered around walk-trot gaits. The reduction of musculoskeletal forces has been studied in the context of the trot-gallop gait transition in horses, particularly at high velocities⁶. However, for the walk and trot gaits at normal velocities, critical peak contact forces are not significantly present.

Qualitative comparison of robot and animal data for locomotion on flat terrain

We examine the consistency of our hierarchical biology-inspired learning architecture with animal locomotion experiments performed by Granatosky et al. which characterized how gaits, energy efficiency, and periodicity depend on speed⁷. Granatosky et al. estimated the Cost of Transport (CoT) based on oxygen consumption: the lower the CoT, the higher the energy efficiency. They computed periodicity from the Coefficient of Variation (CV) of the stride duration: the lower the CV, the higher the periodicity. Figure (2)-A presents results for the first experimental category: walking and trotting for the robot with data from four quadruped animals: domestic dog (*Canis lupus familiaris*), Australian water rat (*Hydromys chrysogaster*), Virginia opossum (*Didelphis virginiana*), and tufted capuchin (*Sapajus apella*). We use second-order polynomial fitting for the CoT as used in Granatosky et al.⁷. The speed at which the CoT curve for a walking gait intersects with the CoT curve for a trotting gait represents the energetically optimal transition speed (EOTS). The EOTS can be found by extrapolating the walking and trotting curves, however there are some cases for which the intersection does not exist, such as for the domestic dog (Figure (2)-b). Moreover, there is limited data available for the Australian water rat, so the extrapolation/interpolation of the fitted curve may not provide definitive information. For both the robot and the animals, switching gaits at the EOTS leads to a reduction in energy expenditure. However, it is important to note that the preferred transition speed does not align exactly with the EOTS for most animals. The domestic dog (b) and Virginia opossum (d) have the most similar CoT curves to the robot. For the robot and all animal species besides the Australian water rat, the CV of the stride cycle duration is reduced by a change in gait. Moreover, in the Virginia opossum (d) and tufted capuchin (e), the CV of the stride cycle duration has a peak near the gait-transition speed.

Figure (2)-B shows the absolute average of Divergent Component of Motion (DCM) offset and average angular velocity of the robot. Increasing the DCM generally corresponds to a more dynamic gait, which in turn increases the risk of falling. We observe that, as with the CV of the stride duration, switching gaits reduces the lateral DCM offset (panel (f)). The desired lateral DCM offset is zero, since the robot is walking forward in a straight line. Increasing locomotion velocity in a given direction fundamentally requires an increase in the DCM offset in that direction. Therefore, the DCM offset in the X direction exhibits a reasonable behavior (panel (g)). Switching gaits also decreases the average body angular velocity (panel (h)), improving stability.

In the second scenario of locomotion on flat terrain, we investigate the data of extended gaits from Hoyt and Taylor². Horses continue to train their motor control through a lifelong learning process to locomote at certain limited speed ranges for each of their gaits². To investigate locomotion principles, horses were briefly trained to extend their gaits to speed ranges in which they would not normally use that gait. During this process, horses learn to increase their velocity by lengthening their stride while maintaining a relatively constant frequency. While horses learn to optimize their motor control policies over a long period of time, they were taught to extend their gaits during a short period, experiencing new locomotion parameters which they had not previously encountered in their lifetime. In the context of robot locomotion, extending a gait can be understood as a scenario in which the robot is forced to locomote at speeds outside of the range optimized for during the training process. Figure (2)-C illustrates the results from the second experimental category: extended walking and trotting gaits for both the robot and horse. Interestingly, the resulting CoT curve shape for the robot is very similar to the data from the horses. Comparing panels (a) and (j) reveals that an extended trot produces a CoT-velocity curve with higher curvature. In other words, the CoT increases rapidly for speeds that are farther from those for which the robot was optimized for (and similarly for the horse, speeds that are farther from those it would choose naturally before the rapid training of extended gaits). Moreover, because we changed the stride length manually in panel (j), the policy experiences states for which it had not been optimized for during locomotion. Thus, the viable range of speeds for panel (j) is smaller than for panel (a).

Emergence of Gait Transitions in Gap Crossing Scenarios

We trained the robot to cross 8 challenging gaps in a row with 14 cm platforms between each gap in the PyBullet simulator (Figure (3)-a). The gaps were randomized in width in the range of [14, 20] cm. As exteroceptive sensory information, we include the distances between each foot and the front and back of the next upcoming gap in the observation space. The base and feet trajectories are shown in Figure (3)-b. We observe that the agent has learned to increase the stride length, maximum feet height, and average body height in order to cross the gaps. Interestingly, Figure (3)-b shows that the robot places its hind limbs where the front limbs were located in the previous stride, similarly to how cats place their rear paws in the pawprints made by their front paws (also known as *direct registering*)⁴⁷. In order to ensure a reliable contact surface near the gaps, the robot places front and hind feet in the same positions once it reaches the gaps. This strategy improves the predictability of the gait, which facilitates the anticipation of the non-viable states and thus increases gap traversing abilities. Figure (3)-c illustrates the duration that each foot is in contact with the ground. We observe a trotting gait prior to reaching the gaps, where diagonally opposite feet (e.g. front right and hind left) are in phase. However when crossing the gaps, the supraspinal drive has learned to transition gaits from trot to pronk, so that all feet are in the same phase. As shown in Figure (3)-d, as the robot starts to cross the gaps, the supraspinal drive increases the robot's velocity. While we limit the reward the agent can receive by setting the desired forward velocity to 1 (m/s), the agent has learned to increase the velocity of the robot to up to 1.5 (m/s) to cross

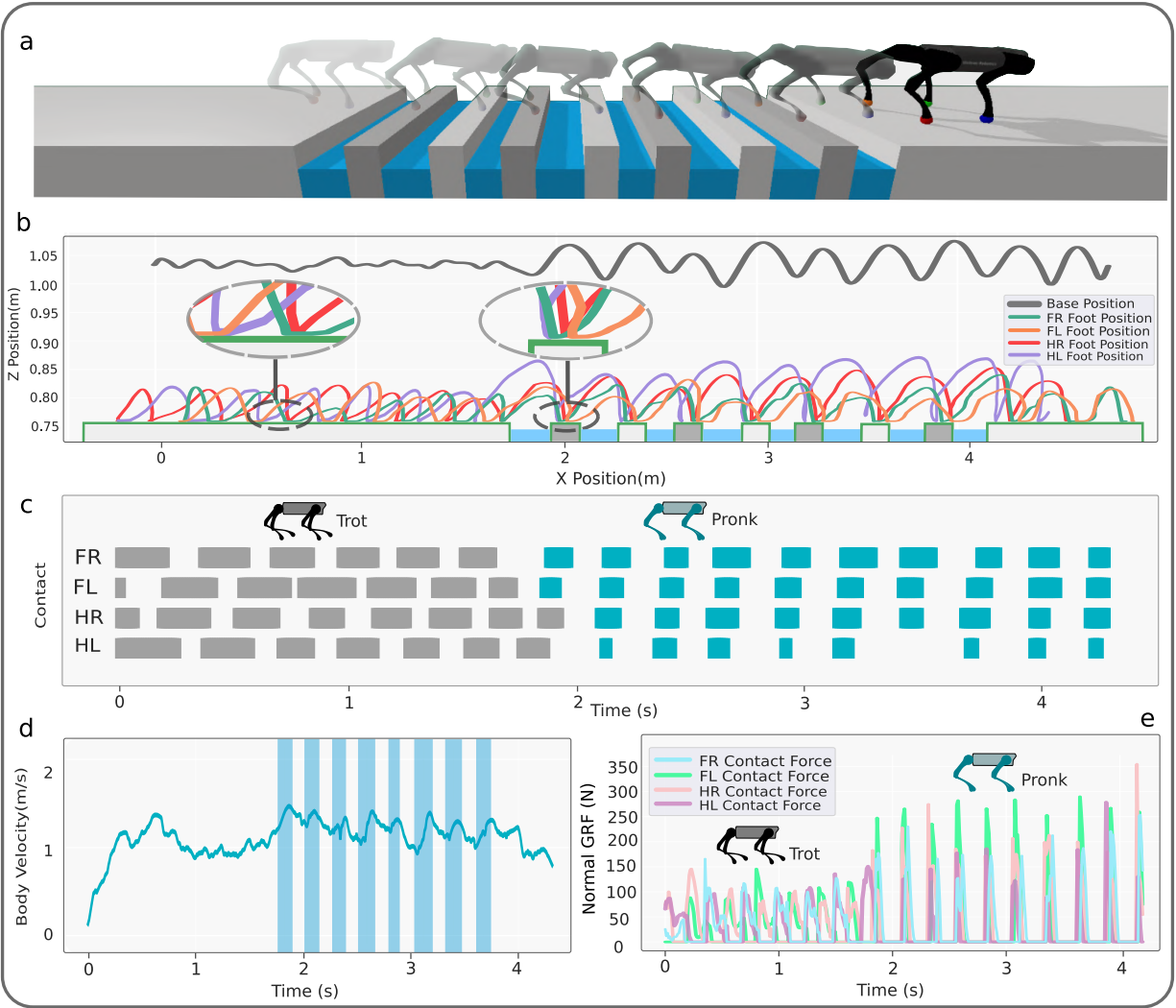


Figure 3. Crossing 8 gaps with randomized lengths between [14, 20] cm, with only 14 cm contact surfaces. **a:** simulation snapshots. **b:** body position and foot positions in the XZ plane. **c:** foot contact duration, where blue represents contacts while crossing the gaps. **d:** body velocity in the longitudinal direction. The shadow bars indicate when the base is over a gap. **e:** Normal contact (ground reaction) forces for each limb. Video link: [\[Link\]](#).

the gaps. Table (1) shows the CV of the stride duration and length, as well as the CoT before and after reaching the gaps and the gait transition. There is a reduction in the CV of the stride duration and stride length after the gait transition, indicating a reduction of the kinematic and dynamic variability. However, the CoT increases after the gait transition, indicating an increase in energy expenditure for the pronk gait. Figure (3)-e shows the normal contact forces for each limb, and in particular the increase of the contact peak forces after the trot-pronk gait transition. These results suggest that, in our experiments, energy efficiency and peak forces do not explain the gait transition, and that it is rather the avoidance of non-viable states that triggers the gait transition, as could be expected from this particular environment.

To analyze the impact of each component of the reward function, we trained 27 policies in Isaac Gym, considering three different values (high, medium, and low) for the reward weights associated with viability, CoT, and contact peak forces. Figure (4) shows the success rate, CoT, and deviation of the contact force from its maximum value threshold across various cases. As exteroceptive sensory information, we include a height-map in front of the robot, beginning below its front hip (see Supplementary Material). Figure (4)-a shows the weights of each case. The highest success rate is obtained with case 19, in which viability, CoT, and peak forces are assigned high, low, and low weights, respectively, as in the PyBullet results. It is noteworthy that this case exhibits the highest success rate of 100% across 2400 gap attempts, and interestingly, the CoT remains approximately constant, while peak forces increase after the gait transition from trotting on flat terrain to pronking over the discrete gap terrain. Case 23, with a high weight for viability and medium weights for CoT and peak forces, achieves

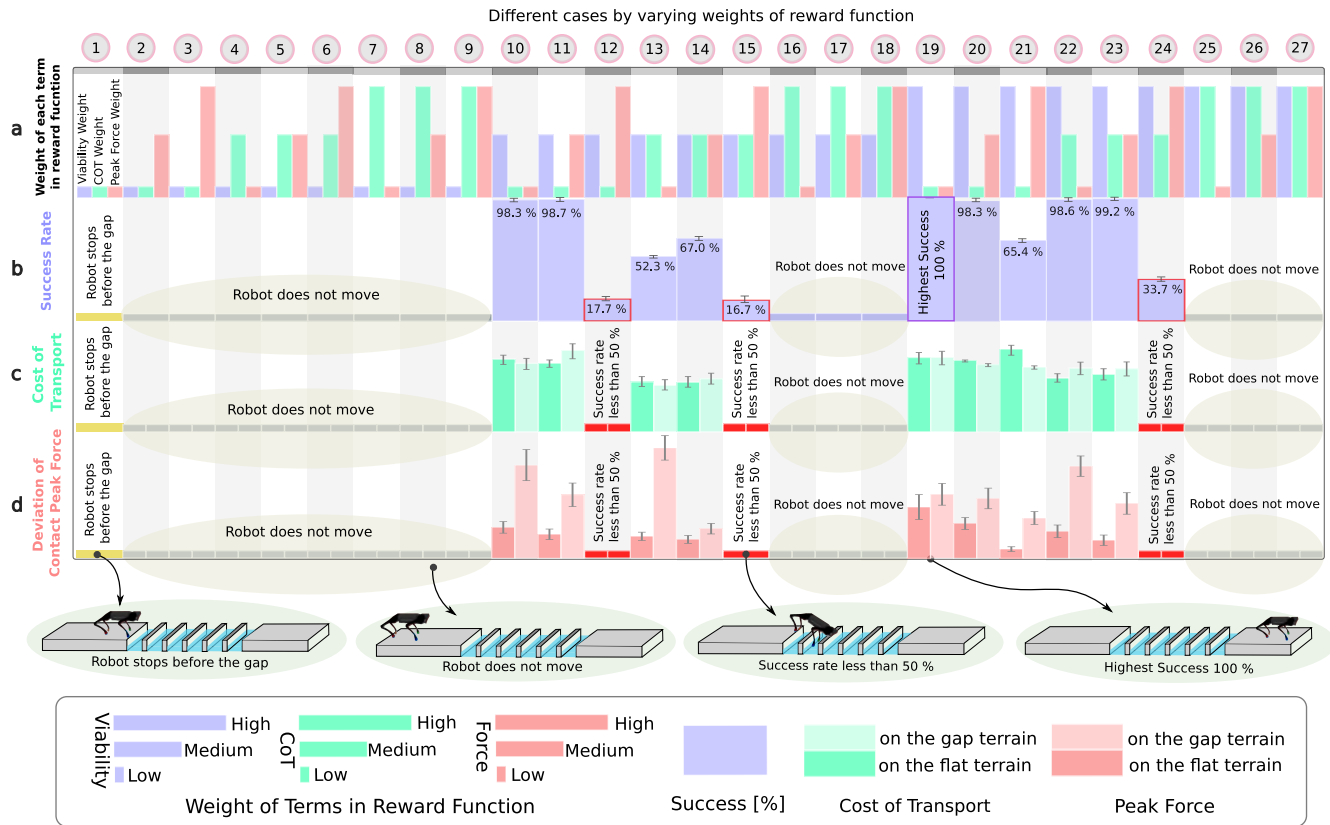


Figure 4. Quantitative results from testing 27 policies with varying weights in reward function for crossing two series of 6 consecutive gaps. We consider three values of low, medium, and high for the weights of the reward function terms for viability, CoT and contact peak forces. The low and medium weights are selected to be approximately 1% and 50% of the high values. We report average success rate, CoT, and contact peak forces for testing the policies for 4400 samples each (200 attempts of crossing 12 gaps). We show mean values and the standard deviations for success rate and Cost of Transport. To evaluate the peak forces, we first separately trained locomotion controllers on flat terrain to reach a velocity of 1.2 m/s, which is the average gap crossing velocity, and observed peak contact forces of 180N. For the gap crossing scenario, our reward function penalizes peak contact forces above this threshold at each control cycle, and the plots show the mean contact force in excess of 180N across all tests. Video link: [\[Link\]](#).

the second highest success rate of 99.2%. However, the CoT and peak contact forces also do not show improvement after the transition. Among cases 10, 11, 20, and 22, which all have a success rate above 98%, it is observed that in two cases the CoT decreases after the gait transition, while in the other two cases it increases. The peak forces increase after the gait transition in all four of these cases. This suggests that the improvement of CoT and peak forces is not necessarily guaranteed after the gait transition. The robot learns to walk with low reward function term values for all weights in case 1; however, it stops before the gap. In cases 2-9, by assigning a low weight to viability and various combinations of medium and high values for the contact peak forces and CoT, the robot remains stationary for the whole episode and does not exhibit any movement. In case 12, where medium and low weights are assigned for viability and CoT, and a high weight is assigned for contact forces, we observe a significant decrease in the success rate compared to cases 10 and 11, which have medium and low weights for contact peak forces. We observe a reduction in the overall CoT in cases 13 and 14, compared to cases 10 and 11. This reduction is attributed to the utilization of a medium weight for penalizing the CoT, albeit at the cost of a decrease in the success rate. In cases 12, 15, and 24, we observe a success rate of less than 50%, with the common characteristic of having a high weight for minimizing peak forces. Cases 16, 17, 18, 25, 26, and 27 fail to learn to move and instead remain stationary due to their high weight for penalizing the CoT. We observe an increase in peak forces in all cases which have a success rate higher than 50%.

Table 1. The CV of the stride duration, stride length, and CoT before and after a gait transition (Figure (3)).

	CV Stride Duration	CV Stride Length	CoT
Before Gait Transition	0.38	0.44	0.84
After Gait Transition	0.31	0.35	0.93

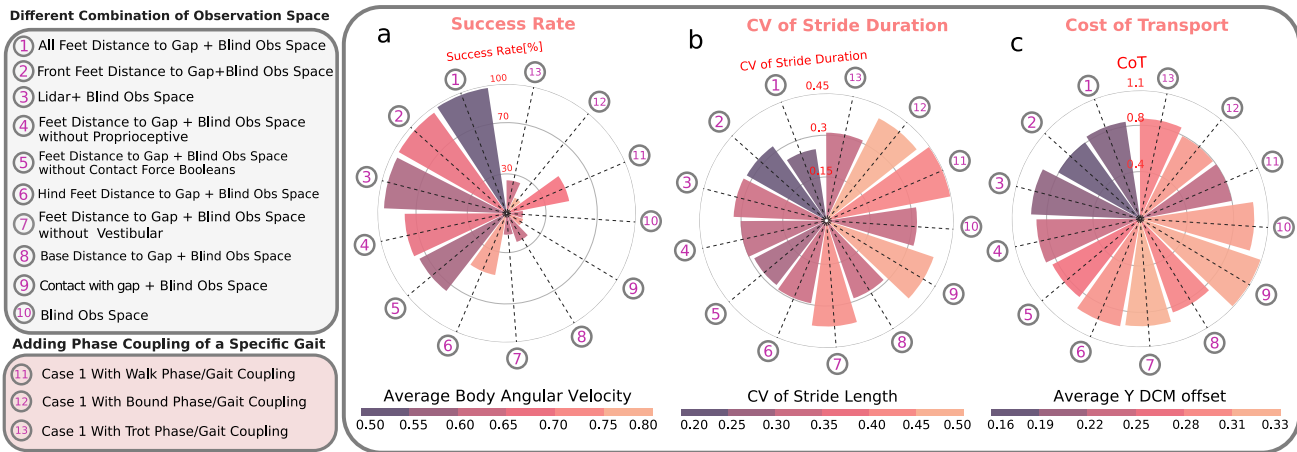


Figure 5. Quantitative results from testing 13 policies with varying observation spaces and phase coupling for crossing a series of four consecutive gaps. We report average success rate, body angular velocity, CV of stride duration/length, Cost of Transport, and lateral DCM offset for testing the policies for 50000 samples each (14 attempts of crossing four gaps). Policies 1-10 are trained using a variety of combinations of “blind” (non-visual) and exteroceptive visual sensing. We only show mean values since the standard deviations are small (i.e. less than 20% of the means). The standard deviations are reported in the supplementary material. Policies 11-13 are trained with oscillator couplings to force walking, trotting, and bounding gaits, respectively. Exteroceptive sensory feedback features include LiDAR measurements, as well as geometrically-extracted quantities such as feet distances to the gap, base distance to the gap, and foot contact/penetration into a gap (visualized in Figure 6-a). Video link: [\[Link\]](#).

The Role of Sensory Features and Oscillator Couplings in Gait Transition

As shown in Figure (5), we investigate the effects of observing different combinations of exteroceptive, proprioceptive and vestibular sensory features for gap crossing scenarios on criteria such as success rate, average angular body velocity, the CV of the stride duration, the CV of the stride length, the Cost of Transport, and the Average Lateral DCM offset. In particular, we study which sensory feature combinations are necessary and sufficient to learn to successfully cross variable gaps, and we analyze the effects through ablation experiments in cases 1-10. We also investigate the effects of adding explicit oscillator coupling between oscillators such that the agent must walk, trot, or bound in cases 11-13. For the purposes of evaluation, we perform 14 policy rollouts, and present average results across all tests. The simulation snapshots are shown in Figure (6)-b.

Figure (5)-a shows the success rate as the bar height, while the color indicates the average body angular velocity. Our results show the highest success rates for policies 1, 2, and 3, which observe (1) the distances of all feet to the gap, (2) the distances only of the front feet to the gap, and (3) LiDAR depth measurements in front of the robot, respectively, in the observation space. The average body angular velocities of these three policies show that they also generate the smoothest gaits. Cases 4 and 5 show that removing contact force booleans and proprioceptive information from the observation space reduces the success rate by approximately 20%. The removal of front-feet distances to the gap in case 6 leads to a 50% reduction in the success rate. Case 7 shows that removing vestibular information (IMU data) from the “blind” sensory information leads to only a 16% success rate. Case 8 shows that sensing base distance to the gap, rather than explicit feet distances to the gap, results in only a 23% success rate. The lowest success rates are for cases 9 and 10, where only instantaneous contact/penetration into a gap, or no gap information at all are included in the observation space. Finally, in cases 11-13, we observe that phase coupling of walking, trotting, and bounding gaits lead to success rates of 48%, 13%, and 25%, respectively, indicating that such couplings that impose a particular gait have a detrimental effect on the success rate. This suggests that supraspinal drive might play an important role in modulating coupling strengths for anticipatory locomotion.

Figure (5)-b shows the CV of the stride duration (bar height) and the CV of the stride length (color). Of the cases with a high success rate, case 1, which includes foot distance to the gap in the observation space, has the lowest CV of stride duration. The CV of the stride duration does not vary significantly between the other cases with high success rates. Cases 1 and 2, with explicit visually-extracted information of feet distances to the gaps, have the lowest CV for the stride length.

Figure (5)-c shows the Cost of Transport (bar height) and average lateral Y DCM offset (color). Of the cases with high success rates (cases 1-3), cases 1 and 2 show that having all/front feet distances to the gap as explicit exteroceptive sensing leads to a lower CoT. The CoTs of the other cases are not as informative, as they have low success rates where the robot frequently falls into a gap. The lowest average lateral DCM offsets are for cases 1 and 2, which include all-feet distances, or only front-feet distances, to the gap in the observation space. These results suggest that front-feet distances to the gap are

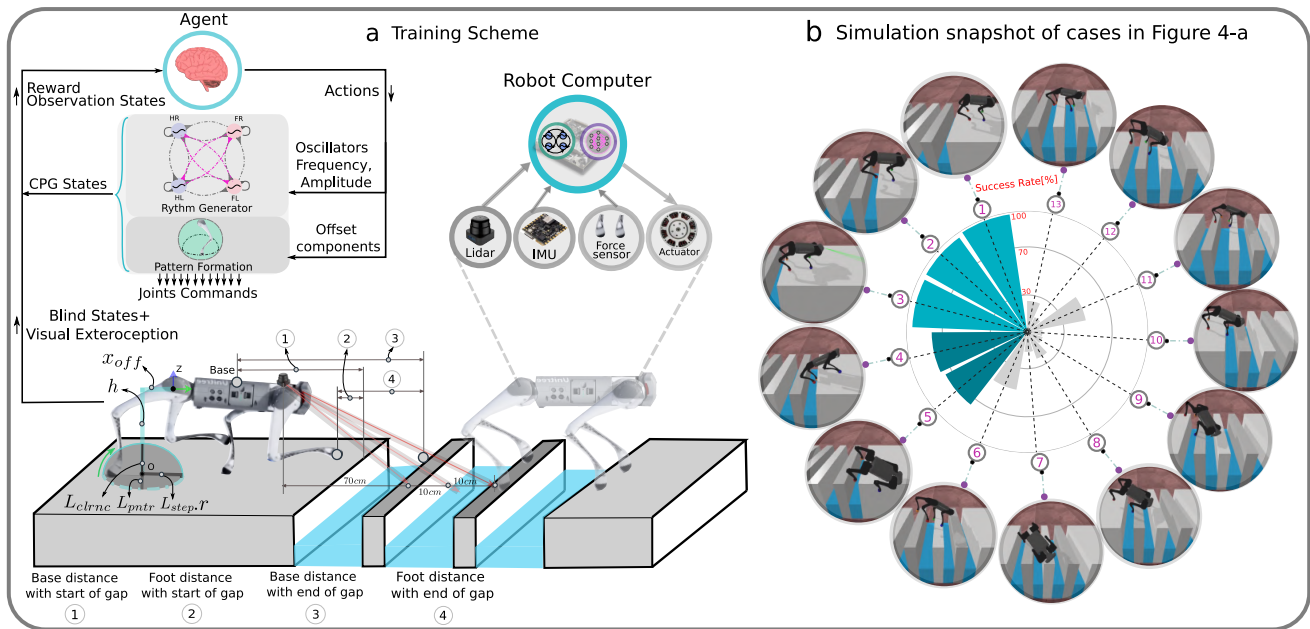


Figure 6. a: Training scheme and schematic visualization of feet trajectory and visual exteroceptive feedback features. The oscillatory trajectory is built around a central point O . The offsets x_{off} are used to change the central point of oscillation. x_{off} is a horizontal offset between the set-point of oscillation and the center of the hip coordinate, controlled directly by the supraspinal drive, bypassing the CPG dynamics. L_{step} is the step length multiplied by the oscillator amplitude, h is the nominal leg length, L_{clrmc} is the max ground clearance during leg swing phase, and L_{pntnr} is the max ground penetration during stance. The desired foot positions are mapped to motor commands and tracked with joint PD control, and sensing includes LiDAR for visual perception, an Inertial Measurement Unit (IMU) to filter base velocities and orientation, and foot contact sensors for measuring contact forces. **b:** Simulation snapshots of cases of Figure 5-a.

necessary and sufficient explicit sensory features to avoid non-viable states (i.e. falling into a gap).

Hardware Experimental Results

Figure 7-a shows snapshots of a sim-to-real transfer to the A1 hardware of a policy trained with our proposed method for a task of crossing four consecutive gaps with widths of 30 cm, 21 cm, 18 cm, 14 cm. We simplify the sim-to-real transfer by using knowledge of the relative gap distances to the robot from an equivalent scenario completed in simulation, instead of using on-board vision or LiDAR. The robot crosses this challenging gap scenario with a velocity of 1.3 m/s, and we observe a trot-pronk gait transition when reaching the gaps, and a pronk-trot gait transition after crossing the last gap.

Table 2 compares the performance of the proposed bio-inspired controller with other quadruped robot controllers for gap-crossing scenarios. The proposed controller outperforms the previous state-of-the-art controllers by showing the ability to cross the most challenging consecutive gaps of up to 30 cm (0.83 gap/body length ratio), with only 14 cm beam contact widths between gaps. Furthermore, our hierarchical biology-inspired policy generates the most agile gap crossing with a velocity of 1.3 m/s. These results suggest that a better understanding of animal behavior through testing biological hypotheses with robots can help improve robot locomotion performance.

Discussion

We began this study by evaluating the consistency of the locomotion policies learned with our framework with available animal data for walking and trotting on flat terrain. The CoT and CV of the stride duration were found to be qualitatively consistent across both considered categories of animal experiments and robot simulations, namely walking and trotting with and without extended gaits. Furthermore, we investigated why the CoT-velocity curve for trotting has a higher curvature for the second category of animal experiments, concluding that the difference is mainly attributable to the extension of gaits in these experiments. We simulated extended gaits by varying the stride length, taking inspiration from previous horse experiments⁵⁸. More specifically, once we had trained walking and trotting gaits at particular velocities, we manually altered the stride length mapping parameter in order to achieve locomotion at velocities outside of those trained for with the same gait. We observed that the CoT of the extended gaits increased rapidly as the robot velocity moved away from its optimal point for both robots and

Table 2. Comparison of the DeepTransition gap-crossing controller with state-of-the-art methods (hardware results)

Research	Robot - Year	Gap	$\frac{\text{Max Gap width}}{\text{Body length}}$	Beam width	Speed [km/h]	Froude	Controller
Kalakrishnan et al. ⁴⁸	Little Dog - 2011	Single gap	0.772	N/A	0.385	0.007*	Optimization
Magana et al. ⁴⁹	HYQ - 2019	Consecutive	0.135	20 cm	1.8	0.046	Optimization
Yu et al. ⁵⁰	Laikago - 2021	Single gap	0.4	N/A	1.35	0.032	MPC-RL
Lee et al. ⁵¹	Laikago - 2022	Single gap	0.4	N/A	1.35	0.032	MPC-RL
Agarwal et al. ⁵²	Unitree A1 - 2022	Consecutive	0.72	30* cm	1.26	0.041	RL-Supervised
Xie et al. ⁵³	Unitree A1 - 2022	Single gap	0.41*	N/A	1.08	0.03*	RL-Optimization
Agrawal et al. ⁵⁴	Unitree A1 - 2022	Consecutive	0.5	20 cm	0.9	0.021	Optimization
Margolis et al. ⁵⁵	Mini-Cheetah - 2022	Single gap	0.4	N/A	4.5	0.549	MPC-RL
Rudin et al. ⁵⁶	ANYmal C - 2022	Single gap	0.9*	N/A	3.6*	0.203*	RL-Curriculum
Yang et al. ⁵⁷	Unitree A1 - 2023	Single gap	0.83	N/A	1.44	0.054	RL-Supervised
DeepTransition	Unitree A1 - 2023	Consecutive	0.83	14 cm	4.68	0.574	CPG-RL

Consecutive gaps corresponds to scenarios where the robot crosses multiple gaps in a row with small distances between gaps (the distance between gaps is less than the body length). The beam width indicates the distance between the gaps. We do not report beam width for the single gap scenario since there is considerable distance (more than body length) between gaps. The Froude number ($v^2/(g \cdot h)$) is a dimensionless number that is useful for size-independent comparisons of animal and robot agility. (g), (v) and (h) are gravity acceleration, forward velocity, and nominal base height respectively. * denotes an estimation from the corresponding publication video.

horses. For this reason, the curvature is greater in this case than in the first category of data, which did not include extended gaits. We hypothesize that the large increase in CoT in relation to the changing velocity can be explained by the fact that the locomotion policies of both the animals and robots have not been optimized for these parameters. Our findings suggest that a quadruped robot can be a useful tool for testing biological hypotheses about quadruped animals.

In the second part of this study, we tested whether viability can be a determinant of gait transitions in quadruped locomotion, concluding that gait transitions can be triggered by environment perception to avoid unviable states in challenging terrain. We can make the following observations:

- In situations where the robot was constrained to locomote by walking, trotting, or bounding gaits, it was unable to learn to solve challenging gap crossing scenarios with a high success rate. This observation suggests that the trot-pronk transition emerges to prevent the robot from falling into gaps and to prevent non-viable states.
- Our systematic analysis of the reward function term weights for viability, CoT, and peak forces demonstrates that viability is the most critical term to accomplish successful gap crossing, and high weights for penalizing the CoT and/or peak forces results in an inability to learn gap crossing abilities. This finding highlights the significance of viability in the locomotion task.
- Energy efficiency and peak forces have not necessarily been improved after the trot-pronk gait transition, which shows that, in our case, a gait transition is not triggered in order to reduce energy expenditure, and while the pronk gait can serve as a way to cross gaps, it may also increase the risk of injury to the body (musculoskeletal system). The CV of the stride length is reduced by the transition from trot to pronk, which shows that following the gait transition, the predictability of the gait increases.
- From all tested exteroceptive sensory features, the highest gap crossing success rate was found for policies which included feet distances to the gap in the observation space. This information can be directly used by the policy to forecast and anticipate planning future footstep locations. In particular, we observe that front-feet distances to a gap are the most important exteroceptive sensory features, which are both necessary and sufficient explicit features for learning to cross gaps.
- If the only exteroceptive sensing the agent has access to are the front feet distances to a gap, this forces the agent to learn an internal kinematic model by combining front foot position, internal CPG states, and proprioceptive sensing to modulate the “blind” hind leg motions to successfully cross the gaps. This result corroborates the hypothesis that cats and horses control their front legs for obstacle avoidance, and that their hind legs follow the previous support location of the front legs based on internal kinematic memory^{47,59}. This is also known as *direct registering*. Similarly, our robot places its hind limbs approximately where the front limbs were located in the previous stride, which enhances gait predictability by lowering the CV of the stride length. However, it is worth noting that the CV of the stride length must increase when crossing irregular gaps.

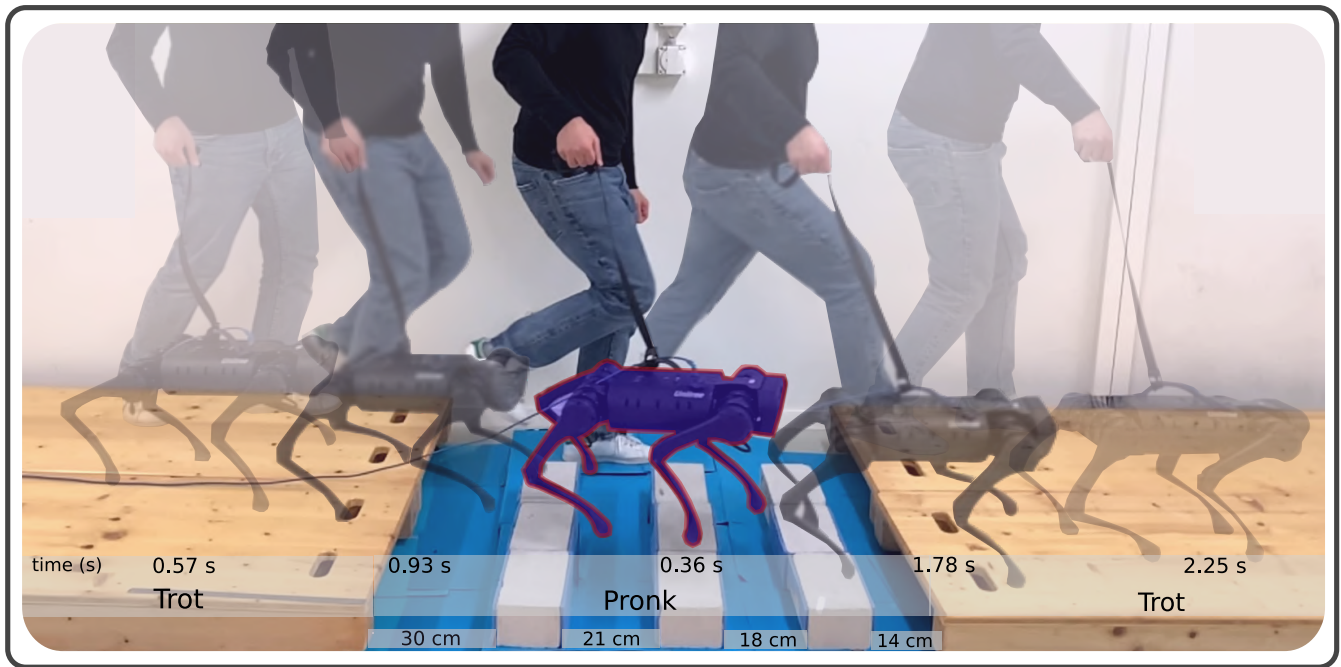


Figure 7. Crossing four gaps with widths of 30 cm, 21 cm, 18 cm, and 14 cm with a velocity of 1.3 m/s. We observed the emergence of a trot-pronk gait transition when approaching the gaps, followed by a pronk-trot gait transition after successfully crossing the last gap. Video link: [\[link\]](#).

- Finally, our results suggest that vestibular feedback has a high impact on viability in the emergence of trot-pronk gait transitions in our designed gap crossing scenarios. A previous study suggests that vestibular feedback has the greatest impact on the landing behavior of cane toads⁶⁰. In our study, the landing phase is the most challenging phase of the emerged pronk gait as the agent must control and plan footholds and body orientation to avoid falling into a gap, and our results support that vestibular sensing has a high impact on successful landing. For example, Case 7 of Figure 5 shows a drastically reduced success rate when removing vestibular information from the observation space.

Several previous biological studies have suggested that gait stability can be considered as a primary determining factor for gait transitions of quadruped animals on flat terrain^{7,32,61}. These studies suggested that CoT may be used as a surrogate for gait stability or as a secondary objective. In this paper, we propose viability as a comprehensive criteria for gait transitions, for which gait stability is a subset. In particular, our simulation results in the anticipatory scenario propose that viability is the primary objective for the emergence of gait transitions on variable discrete terrains. These observations suggest viability is the universal and primary objective of gait transitions, while other criteria are secondary objectives and/or a surrogate of viability.

We believe that this paper represents a useful starting point for using robots and deep learning to investigate the determinants and triggers of gait transitions. There is, however, much room for further investigation. For example, the nonlinear oscillators are only first-order approximations of CPG circuits and are useful for investigating neuroscience research questions at a high level. However, a more detailed understanding of the underlying circuits (for example for identifying the descending pathways that contribute to gait transitions) would require more detailed and genetically-identified models for CPG neural circuits⁶².

The dynamics of the musculoskeletal system also play a key role in the robustness and energy efficiency of animal locomotion. We therefore plan to incorporate a simulation of the animal musculoskeletal system (for example with pairs of antagonist muscles, as well as biarticular muscle models) and investigate its role for gait transitions. As mentioned earlier, there is evidence that gait transitions may occur to reduce the mechanical load on the musculoskeletal system and joints⁶. We believe that our framework will provide a useful tool for investigating this problem, by directly penalizing the muscle peak forces and joint jerk in our reward function, and using these values as feedback to the CPG or as a part of the observation space. Additionally, it has been suggested that contact loading feedback to the CPG can trigger the gait transition by increasing locomotion frequency and speed on flat terrain^{28,29}. By incorporating contact loading feedback to the CPG, the proposed architecture can be extended to investigate the interaction between supraspinal drive and loading feedback for triggering gait transitions on flat terrain.

Methods

Locomotion Metrics

Viability: In control theory, Lyapunov stability of an equilibrium point means that solutions starting within some distance from the point will remain “close enough” forever. Any perturbations will lead only to minor and transient changes for the state variables of a stable system. Mathematical tools for dynamical systems can be used to analyze gait transition stability³², however they are limited to the internal dynamics of the system without considering environmental constraints. For example, a robot may have a stable gait (in the sense of Lyapunov stability), but still fall when it steps into an unanticipated gap. Legged locomotion, when trying to maintain balance and avoid such falls or collisions with obstacles, can be considered to be a problem of *viability* rather than Lyapunov stability⁴⁵. If F is the set of states in which the system is considered to have fallen, then the viable states are the set of states from which the robot can avoid entering F (see Figure S.3.1 in the supplementary material)⁴⁴. In this article, we use “viable states”, rather than “stable states”, to fully capture the concept of fall prevention in legged locomotion.

On variable terrains with discrete footholds, a robot can fall by stepping into a gap, thereby entering a non-viable state. Unfortunately, in general the computation of the viability kernel can be intractable (except for the simplified pendulum model^{63,64}), and due to the complexity of the multi-body dynamics of walking systems, it may be numerically extremely expensive or even impossible to check whether a given state is viable or not⁶⁵. However, when learning gap crossing skills, it is possible to define the reward function such that it promotes not entering into non-viable states (stepping into a gap), and thus promotes viability. Viability can also be indirectly evaluated by considering the success rate of traversing variable environmental conditions, for example the number of gaps that the robot is able to successfully cross out of the total number of gaps encountered.

Griffin et al.⁶¹ hypothesized that horses transition gaits from walking to trotting on flat terrain based on the stability of the inverted pendulum dynamics. On flat terrain, the viability of locomotion based on the linear inverted pendulum model (LIPM) approximation can be evaluated based on the Divergent Component of Motion (DCM) offset^{66,67}. The DCM (also called Capture Point or Extrapolated CoM) dynamics is the unstable component of the LIPM, and the DCM offset (distance between the DCM and the Center of Pressure (CoP)) specifies the rate of divergence for the unstable component (see the supplementary material). The DCM offset becoming greater than a certain threshold will lead to entering non-viable states, and this threshold can be calculated for bipedal locomotion assuming a single support phase⁶⁸. Although this does not apply to quadrupedal locomotion, we can still use the DCM offset as an indicator of approaching the boundary of the viability kernel. In our experiments, the desired lateral motion is zero, and therefore an increase in the lateral DCM offset corresponds to a reduction in viability.

Stride Duration Variability (Periodicity): We propose that viability on flat terrain can also indirectly be evaluated by inter-stride variability. Indeed, locomotion gaits with high inter-stride variability, increase the risk of inter-limb interference, making tripping and/or falling more likely on flat terrain. Therefore, variability in inter-stride parameters has important biomechanical consequences for gait stability^{7,69}. This variability can be computed by the Coefficient of Variation (CV), which is defined as the ratio of the standard deviation to the mean of the data, and indicates the variability. We compute the CV of the stride duration for whole strides in one episode, and use this quantity to evaluate viability on flat terrain (but not on irregular terrain). On regular uneven terrain such as structured gaps, periodicity exhibits a direct relationship with viability. A higher level of periodicity corresponds to greater consistency with the terrain. However, in irregular terrain, periodicity does not necessarily enhance viability.

Stride Length Variability (Predictability): The CV of the stride length is used to evaluate the predictability of a locomotion gait. A low stride length CV means that the stride length is relatively constant, and that the next step position can be predicted based on previous steps. Predictability of a gait therefore simplifies the anticipation of future feet placements. Similar to periodicity, predictability is advantageous in the case of regular and structured terrain. The CV is calculated for all whole strides by all limbs during a training episode, and the mean is then calculated over all episodes.

Energy Efficiency: We compute energy efficiency for a system with the dimensionless Cost of Transport (CoT). The CoT formula is defined as $CoT = \frac{P}{m \cdot g \cdot v}$, where P is the average power, v is the average velocity, m is the mass of the system, and g is the gravitational acceleration.

Gait Smoothness: To evaluate gait smoothness, we analyze the robot body oscillations during locomotion, and in particular the average angular velocity of the robot body $\bar{\omega}_{Body} = (\sum_{t=1}^N (|\omega_{x,t}| + |\omega_{y,t}| + |\omega_{z,t}|)) / (3N)$. High (absolute) angular velocities tend to correspond to shaky gait patterns.

Peak Force: We evaluate *peak force* by measuring the peak ground reaction force. We use this as a proxy for representing peak forces that an animal would experience in its joints and muscles.

Data from Previously Performed Animal Experiments

We assess the consistency of our learning architecture via a qualitative comparison with animal data on flat terrain, which involves plotting the CoT and the coefficient of variation (CV) of the stride duration against locomotion speed. We use two categories of animal data collected in previous studies.

Normal Gaits on Flat Terrain: The first data category includes locomotion data from a study by Granatosky et al.⁷ from which we use data from quadrupeds of various species such as Virginia opossums (*Didelphis virginiana*), tufted capuchins (*Sapajus apella*), domestic dogs (*Canis lupus familiaris*), and the American mink. Animals in this category locomote in a wide range of speeds, which correspond to different specific gaits. The animals were trained to sustain six to ten minutes of steady-state locomotion at any given speed, as required for metabolic measurements. A transition between walking and trotting gaits was observed by placing the animal onto an enclosed treadmill and incrementally increasing the speed of the moving belt every 15 s. The data has been extracted from the supplementary material of Granatosky et al.⁷

Extended Gaits on Flat Terrain: The second category comprises data from a study by Hoyt and Taylor² for walking and trotting gaits for horses, which we extracted from Figure 2² using the WebPlotDigitizer online tool⁷⁰. For given speed ranges, horses tend to locomote with a specific gait (i.e. walking at low speeds, trotting at medium speeds, and galloping at high speeds). However, in these experiments², horses were taught to extend their gaits for a wider range of speeds. For example, an *extended trot* is defined as a situation where a horse continues to trot at speeds above or below its normal trotting speed⁵⁸. This is in contrast with the first category of data, where there is no gait extension and the animals locomote with their nominal gaits at all speeds.

Central Pattern Generators

The locomotor system of vertebrates is organized such that the spinal Central Pattern Generators (CPGs) are responsible for producing basic rhythmic patterns, while higher-level centers (i.e. the motor cortex, cerebellum, and basal ganglia) are responsible for modulating the resulting patterns according to environmental conditions¹. Rybak et al.⁷¹ have proposed that biological CPGs typically have a two-level functional organization, with a half-center rhythm generator (RG) that determines movement frequency, and pattern formation (PF) circuits that determine the exact shapes of muscle activation signals. Similar organizations have also been used in robotics, for example in^{72,73}. Here we reuse the controller presented in^{46,72}.

Rhythm Generator (RG) Layer

We employ amplitude-controlled phase oscillators to model the RG layer of CPG circuits in the spinal cord, as they are able to modulate the output signal by changing a few decision variables²⁵:

$$\dot{\theta}_i = \omega_i + \sum_j r_j w_{ij} \sin(\theta_j - \theta_i - \phi_{ij}) \quad (1)$$

$$\dot{r}_i = \alpha \left(\frac{\alpha}{4} (\mu_i - r_i) - \dot{r}_i \right) \quad (2)$$

where r_i is the amplitude of the oscillator, θ_i is the phase of the oscillator, μ_i and ω_i are the intrinsic amplitude and frequency, α is a positive constant representing the convergence factor. Couplings between oscillators are defined by the weights w_{ij} and phase biases ϕ_{ij} . We use one oscillator for each limb.

Pattern Formation (PF) Layer

To map from the RG states to joint commands, we first compute corresponding desired foot positions, and then calculate the desired joint positions with inverse kinematics. This represents the Pattern Formation (PF) layer, and the desired foot position coordinates are formed as follows:

$$x_{i,\text{foot}} = x_{\text{off},i} - L_{\text{step}}(r_i) \cos(\theta_i) \quad (3)$$

$$z_{i,\text{foot}} = \begin{cases} -h + L_{\text{clrc}} \sin(\theta_i) & \text{if } \sin(\theta_i) > 0 \\ -h + L_{\text{ptr}} \sin(\theta_i) & \text{otherwise} \end{cases} \quad (4)$$

where L_{step} is the step length, h is the nominal leg length, L_{clrc} is the max ground clearance during swing, L_{ptr} is the max ground penetration during stance, and x_{off} is a set-point that changes the equilibrium point of oscillation in the x direction. Modulating the foot horizontal offset x_{off} represents direct supraspinal control of the general position of the limb, bypassing the rhythm generation layer. A visualization of the foot trajectory is shown in Figure 6-a.

Interactions Between the Supraspinal Drive and the Central Pattern Generator

We use our hierarchical biology-inspired learning framework^{46,72} for learning locomotion, as shown in Figure (1) and Figure (6)-a. We have used the proposed scheme on flat terrain⁷², as well as on a simple gap crossing scenario⁴⁶. In this paper, we address the challenge of traversing consecutive gaps with small distances between them. Additionally, we explore the use of a height map around the robot in the observation space as an alternative to relying solely on explicit exteroceptive sensory features. The action space remains consistent with the simple gap-crossing scenario⁴⁶. We extend and analyze the reward function, and in particular perform a systematic analysis on the importance of incorporating terms for viability (and velocity tracking terms), Cost of Transport, and peak contact forces. We formulate the supraspinal controller as an artificial neural network (ANN) which is trained with deep reinforcement learning (DRL) to modulate the Central Pattern Generator (CPG) intrinsic frequencies, amplitudes, and offsets of oscillation for each limb to coordinate and produce anticipatory behavior. The problem is represented as a Markov Decision Process (MDP), and we describe each of its components below. To train the policies, we use Proximal Policy Optimization (PPO)⁷⁴, a state-of-the-art on-policy algorithm for solving the MDP. Additional details can be found in the supplementary material.

Action Space

We consider one RG layer for each limb based on Equations (1) and (2), where the RG output will be used in a PF layer to generate the spatio-temporal foot trajectories in Cartesian space (Equations (3) and (4)). Couplings between oscillators are known to exist in biological CPGs for coordinating gaits, but recent work has shown that they might be weaker than previously thought^{26,28}, and that sensory feedback and descending modulation might play an important role in inter-oscillator synchronization. We therefore investigate explicit coupling within the CPG dynamics, as well as implicit coupling through descending modulation from the supraspinal drive.

Flat Terrain: On flat terrain, our action space modulates the intrinsic amplitudes and frequencies of each oscillator which together forms the CPG, by continuously tuning μ_i and ω_i for each leg. We implement oscillator couplings representing both walking and trotting gaits through phase bias matrices (Φ) and coupling strengths ($w_{ij} = 1$). This coupling imposes a specific phase lag between oscillators and therefore constrains the policy to modulate parameters in order to locomote with these specific gaits.

Gap Crossing: For gap crossing scenarios, we do not consider explicit oscillator couplings ($w_{ij} = 0$), with the intuition that the terrain may prohibit certain gaits, and inter-limb coordination should thus be managed through the supraspinal drive. For gap crossing, in addition to modulating μ_i and ω_i , we also consider modulating the oscillation set-points by learning x_{off} . Thus, our action space for gap-crossing can be summarized as $\mathbf{a} = [\boldsymbol{\mu}, \boldsymbol{\omega}, \mathbf{x}_{off}] \in \mathbb{R}^{12}$. We divide the descending drive modulation into two categories: oscillatory components of the CPG dynamics $\mathbf{a}_{osc} = [\boldsymbol{\mu}, \boldsymbol{\omega}] \in \mathbb{R}^8$ and offset components $\mathbf{a}_{off} = [\mathbf{x}_{off}] \in \mathbb{R}^4$ which bypass the CPG dynamics, as in Equations (1)-(4).

Observation Space

We consider two different observation space types based on (1) “blind” sensory information (enough for locomotion on flat terrain) and (2) also including exteroceptive anticipatory sensing for gap-crossing scenarios. We investigate visual exteroceptive information coming from several categories: (1) directly using visual depth information (i.e. LiDAR), (2) visually-extracted geometrical information (i.e. foot distance to a gap), and (3) instantaneous feedback features (i.e. foot “penetration” into a gap). We investigate various combinations of these exteroceptive anticipatory features to understand the roles and importance of different sensory quantities to successfully cross variable gaps.

Blind (Flat Terrain) Observation: For locomotion on flat terrain, we consider sensory information that a “blind” agent could use to coordinate locomotion, in parallel with recent robotics works using DRL to learn legged locomotion^{37,72}. This information includes *vestibular sensory information* (body orientation, body linear and angular velocity), *proprioceptive sensory information* (joint positions and velocities), foot contact booleans, the action chosen at the previous control cycle by the policy network, the internal CPG states $\{\mathbf{r}, \dot{\mathbf{r}}, \boldsymbol{\theta}, \dot{\boldsymbol{\theta}}\}$, and the desired velocity command.

Exteroceptive-Visual Information: We consider two different methods for directly visually querying the surrounding environment. For the first method, we mount a LiDAR sensor at the front of the robot to return depth measurements along three channels (i.e. in PyBullet⁷⁵, Figure 6-a). We also consider querying the terrain heights within an area around the robot base, which can be constructed by geometrically transforming depth camera measurements from a camera mounted at the front of the robot (i.e. in Isaac Gym⁷⁶).

Exteroceptive-Explicit Feedback Features: We assume that the visual system and brain can extract important geometrical information such as foot distance to a gap, and we call such information *exteroceptive explicit feedback features*. We are interested in investigating which explicit exteroceptive feedback features are most useful for the emergence of anticipatory locomotion skills. To reverse engineer this process, we divide the explicit sensory features into two categories: *predictive* and *instantaneous* feedback features. *Predictive* features consist of foot distance and/or base distance to the beginning and end of a gap. *Instantaneous* feedback features consist of boolean indicators of stepping into a gap (foot contact/penetration into the gap).

Reward Function

We consider two locomotion scenarios: 1) steady-state locomotion on flat terrain with oscillator phase coupling for walking and trotting gaits, and 2) gap-crossing scenarios without oscillator coupling. To study the potential determinants of gait transitions, we propose a reward function that encompasses the following components in its general form:

- *Viability*: We promote viability by rewarding forward progress without falling. Locomotion speed during forward progress can be controlled by limiting (or penalizing) the reward for speeds above a maximum velocity threshold, or including a velocity tracking component. For the gap crossing scenario, we utilize the first approach, whereas for flat terrain locomotion, we employ the latter. Velocity tracking is implemented for flat terrain, as it necessitates running the policy at various velocities to measure the CoT. Accurately tracking a desired velocity promotes viability, as it ensures that the robot has not fallen while maintaining the desired task velocity. It is worth noting that the velocity tracking term is added to the forward progress term for flat terrain. For detailed information, please refer to the supplementary file.
- *Cost of Transport*: We penalize power in order to find energy efficient gaits. It is worth noting that, since the average velocity achieved by the robot remains consistent across all simulations, the CoT and power are roughly proportionally equivalent in these cases.
- *Peak force*: We penalize peak contact reaction forces in order to minimize body peak forces during locomotion.
- *Base orientation penalty*: We penalize body orientation deviations from a nominal horizontal position.

The importance of each component can be regularized by changing the weights. We systematically analyze the effects of the reward function by considering three values of low, medium, and high for the reward term weights for viability, CoT, and peak forces in gap-crossing scenarios. The low and medium weights are selected to be approximately 1% and 50% of the high value. Among all 27 possible combinations of low-medium-high for viability, CoT, and peak forces, the highest success rate is observed for the case with the highest viability and lowest CoT and peak contact force weights. We use high and low weight for the viability and energy efficiency terms for flat terrain locomotion. We do not incorporate the peak force component in the reward function for blind locomotion as our investigation on flat terrain focuses on walk-trot gaits. The reduction of musculoskeletal forces has been studied in the context of the trot-gallop gait transition in horses, particularly at high velocities⁶. However, for the walk and trot gaits at normal velocities, there is no significant presence of contact peak forces. The detailed weights of the reward function for each simulation result can be found in the supplementary material.

Training Locomotion Policies on Flat Terrain

On flat terrain, we train separate policies to learn specific gaits (walk and trot) by changing the oscillator phase coupling matrices (Φ) and setting the coupling strength ($w_{ij} = 1$) in Equation (1). We assume that the supraspinal drive does not bypass the CPG dynamics to directly actuate joints in steady-state locomotion, so we do not modulate the offset components ($x_{off,i} = 0$) in Equation (3). We use the *blind (flat terrain) observation space* for these experiments. We also define two separate training conditions regarding the two categories of animal data:

Normal Gait on Flat Terrain

We train policies to test a wide range of speeds (i.e., $[v_{des,min}, v_{des,max}] = [0.3, 1.0] \frac{m}{s}$ for walking and $[v_{des,min}, v_{des,max}] = [0.9, 2.1] \frac{m}{s}$ for trotting) by resampling the desired velocity at the beginning of each environment reset. In order to ensure that the locomotion velocity varies in line with the stride frequency⁷, the upper bound of the CPG frequency in the action space is expressed as a function of the desired velocity. Therefore, our action space limits are $\mu \in [0.5, 4]$, $\omega \in [0, f(v_{des})]$ ($\frac{rad}{s}$), where $f(v_{des})$ is a linear function of the desired velocity:

$$f(v_{des}) = \frac{\omega_{max,2} - \omega_{max,1}}{v_{des,max} - v_{des,min}} * (v_{des} - v_{des,min}) + \omega_{max,1} \quad (5)$$

We use $\omega_{max,1} = 23$, $\omega_{max,2} = 60$ ($\frac{rad}{s}$) to train the walking policy, and $\omega_{max,1} = 30$, $\omega_{max,2} = 70$ ($\frac{rad}{s}$) to train the trotting policy. Therefore, at each episode, the upper bound of allowable frequencies is determined based on the desired velocity.

Extended Gait on Flat Terrain

Biological studies have shown that horses continue to train and optimize their motor control through a lifelong learning process to locomote at certain limited speed ranges for each of their gaits². To investigate locomotion principles, Hoyt and Taylor briefly trained horses to extend their gaits to speed ranges in which they would not normally use that gait² (i.e. trotting above/below their “usual” speed ranges). In order to increase their locomotion speed in an extended gait, the horses learned to increase their stride length. However, their stride frequencies remained approximately constant⁵⁸. While horses learn to optimize their

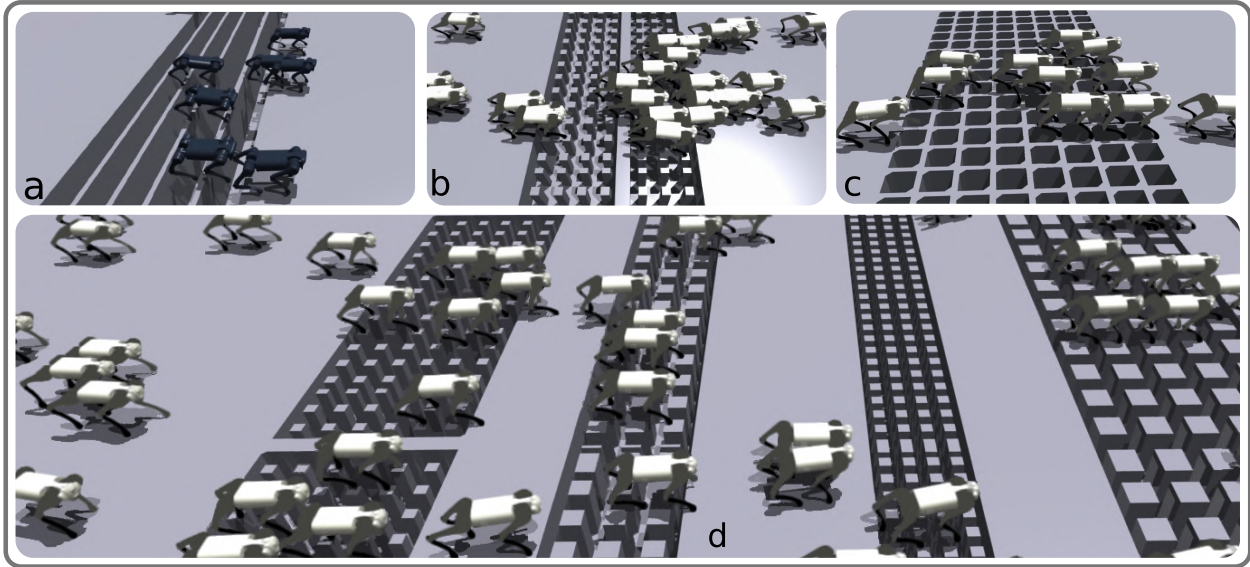


Figure 8. a-d: Training gap-crossing locomotion policies with different robots (Unitree A1, panel a, and Go1, panels b-d) on various discrete terrains in Isaac Gym. Video links: [\[Link a\]](#), [\[Link b\]](#), [\[Link c\]](#), [\[Link d\]](#).

motor control policies over a long period of time, they were taught to extend their gaits during a short period, experiencing new locomotion parameters which they had not previously encountered in their lifetime.

In the context of robot locomotion, extending a gait can be understood as a scenario in which the robot is forced to locomote at a speed for which it was not optimized for during the training process. To simulate experiments in this category, we trained two locomotion policies for certain limited speed ranges (i.e., $[0.4, 0.5] \frac{m}{s}$, for walking, and $[0.85, 0.95] \frac{m}{s}$ for trotting). To match the horse extended gait scenarios, we replicated the experiments with the robot by manually altering the stride length parameter (L_{step} in Equation 3) after training was complete, in order to increase or decrease the velocity. As a result, the policy observed parameter combinations in experiments with this new mapping which it had not encountered during the training process.

Training Locomotion Policies for Gap Crossing Scenarios

We investigate the robot’s ability to learn to cross challenging terrains with multiple consecutive gaps. To allow the agent to coordinate behavior among different limbs through supraspinal drive, we do not consider explicit oscillator couplings ($w_{ij} = 0$ in Equation 1). We use the exteroceptive-visual information in addition to the blind terrain observation space. The action space has the following limits: $\mu \in [0.5, 4]$, $\omega \in [0, 40] (\frac{rad}{s})$, $x_{off} \in [-7, 7]$ cm. The agent selects these parameters at 100 Hz, and they will therefore vary during each step according to sensory data.

In order to evaluate the different locomotion metrics (Figure 5), we perform 14 policy rollouts (50000 samples) on a test environment of locomoting at a desired velocity of 1 m/s over 4 randomized gaps. Each gap length is randomized between $[14, 20]$ cm during both training and test time, with 14 cm contact surface widths between gaps. An episode terminates early because of a fall, i.e. if the body height is less than 15 cm. We define the success rate as the number of gaps successfully crossed out of the total number of gaps. Additional training details can be found in Section S.1.1 of the supplementary material.

We train and test locomotion policies in both the PyBullet⁷⁵ and Isaac Gym⁷⁶ physics engine simulators. PyBullet⁷⁵ limits data collection to one robot per CPU core in our setup, while Isaac Gym⁷⁶ enables data collection from thousands of robots in parallel on a single GPU. Instead of LiDAR, Isaac Gym provides an interface to explicitly query the terrain heights in an area surrounding the robot body, which can be used to provide information about different types of discrete terrains. Figure (8)a-d illustrates various snapshots of the Unitree A1 and Go1 robots locomoting on a variety of discrete terrains, including stepping stones, gap terrains with very small available contact surfaces, grid terrains, and mixtures of each these terrains, respectively. Despite these advantages, the precision of the gap position measurements in Isaac Gym is limited by the constraints of the mesh precision, which are imposed by the available GPU memory. In contrast, PyBullet enables us to easily obtain precise measurements of both the starting and ending positions of a gap. This capability is utilized to investigate the role of explicit exteroceptive sensory features, specifically the measurement of feet/base distance to a gap.

Data availability

Data supporting the findings of this study are available within the paper and its Supplementary Information files. All other relevant data are available from authors upon reasonable request.

Code availability

The code used in this paper is available upon request from the authors.

References

1. Grillner, S. & El Manira, A. Current principles of motor control, with special reference to vertebrate locomotion. *Physiol. reviews* **100**, 271–320 (2020).
2. Hoyt, D. F. & Taylor, C. R. Gait and the energetics of locomotion in horses. *Nature* **292**, 239–240 (1981).
3. Hreljac, A. Preferred and energetically optimal gait transition speeds in human locomotion. *Medicine Sci. Sports Exerc.* **25**, 1158–1162 (1993).
4. Brisswalter, J. & Mottet, D. Energy cost and stride duration variability at preferred transition gait speed between walking and running. *Can. J. Appl. Physiol.* **21**, 471–480 (1996).
5. Tseh, W., Bennett, J., Caputo, J. L. & Morgan, D. W. Comparison between preferred and energetically optimal transition speeds in adolescents. *Eur. journal applied physiology* **88**, 117–121 (2002).
6. Farley, C. T. & Taylor, C. R. A mechanical trigger for the trot-gallop transition in horses. *Science* **253**, 306–308 (1991).
7. Granatosky, M. C. *et al.* Inter-stride variability triggers gait transitions in mammals and birds. *Proc. Royal Soc. B* **285**, 20181766 (2018).
8. Grillner, S. & Zangger, P. On the central generation of locomotion in the low spinal cat. *Exp. brain research* **34**, 241–261 (1979).
9. Brown, T. G. The intrinsic factors in the act of progression in the mammal. *Proc. Royal Soc. London. Ser. B, containing papers a biological character* **84**, 308–319 (1911).
10. Shik, M., Severin, F. & Orlovsky, G. Control of walking and running by means of electrical stimulation of the mesencephalon. *Electroencephalogr. clinical neurophysiology* **26**, 549–549 (1969).
11. Whelan, P. J. Control of locomotion in the decerebrate cat. *Prog. neurobiology* **49**, 481–515 (1996).
12. Grillner, S. & Rossignol, S. On the initiation of the swing phase of locomotion in chronic spinal cats. *Brain research* **146**, 269–277 (1978).
13. Ijspeert, A. J. Biorobotics: Using robots to emulate and investigate agile locomotion. *science* **346**, 196–203 (2014).
14. Li, C., Zhang, T. & Goldman, D. I. A terradynamics of legged locomotion on granular media. *science* **339**, 1408–1412 (2013).
15. Nyakatura, J. A. *et al.* Reverse-engineering the locomotion of a stem amniote. *Nature* **565**, 351–355 (2019).
16. Ijspeert, A. J. Central pattern generators for locomotion control in animals and robots: A review. *Neural Networks* **21**, 642–653, DOI: <https://doi.org/10.1016/j.neunet.2008.03.014> (2008). Robotics and Neuroscience.
17. Yu, J., Tan, M., Chen, J. & Zhang, J. A survey on cpg-inspired control models and system implementation. *IEEE transactions on neural networks learning systems* **25**, 441–456 (2013).
18. Othayoth, R., Thoms, G. & Li, C. An energy landscape approach to locomotor transitions in complex 3d terrain. *Proc. Natl. Acad. Sci.* **117**, 14987–14995 (2020).
19. Spröwitz, A. *et al.* Towards dynamic trot gait locomotion: Design, control, and experiments with cheetah-cub, a compliant quadruped robot. *The Int. J. Robotics Res.* **32**, 932–950, DOI: [10.1177/0278364913489205](https://doi.org/10.1177/0278364913489205) (2013).

20. Ajallooeian, M., Pouya, S., Sproewitz, A. & Ijspeert, A. J. Central pattern generators augmented with virtual model control for quadruped rough terrain locomotion. In *2013 IEEE International Conference on Robotics and Automation*, 3321–3328, DOI: [10.1109/ICRA.2013.6631040](https://doi.org/10.1109/ICRA.2013.6631040) (2013).
21. Aoi, S., Manoonpong, P., Ambe, Y., Matsuno, F. & Wörgötter, F. Adaptive control strategies for interlimb coordination in legged robots: a review. *Front. neurorobotics* **11**, 39 (2017).
22. Kimura, H., Fukuoka, Y. & Cohen, A. H. Adaptive dynamic walking of a quadruped robot on natural ground based on biological concepts. *The Int. J. Robotics Res.* **26**, 475–490 (2007).
23. Thor, M. & Manoonpong, P. Versatile modular neural locomotion control with fast learning. *Nat. Mach. Intell.* **4**, 169–179 (2022).
24. Endo, G., Morimoto, J., Matsubara, T., Nakanishi, J. & Cheng, G. Learning cpg-based biped locomotion with a policy gradient method: Application to a humanoid robot. *The Int. J. Robotics Res.* **27**, 213–228 (2008).
25. Ijspeert, A. J., Crespi, A., Ryczko, D. & Cabelguen, J.-M. From swimming to walking with a salamander robot driven by a spinal cord model. *science* **315**, 1416–1420 (2007).
26. Thandiackal, R. *et al.* Emergence of robust self-organized undulatory swimming based on local hydrodynamic force sensing. *Sci. Robotics* **6** (2021).
27. Dutta, S. *et al.* Programmable coupled oscillators for synchronized locomotion. *Nat. communications* **10**, 1–10 (2019).
28. Owaki, D. & Ishiguro, A. A quadruped robot exhibiting spontaneous gait transitions from walking to trotting to galloping. *Sci. reports* **7**, 1–10 (2017).
29. Fukuoka, Y., Habu, Y. & Fukui, T. A simple rule for quadrupedal gait generation determined by leg loading feedback: a modeling study. *Sci. reports* **5**, 1–11 (2015).
30. Fukui, T., Fujisawa, H., Otaka, K. & Fukuoka, Y. Autonomous gait transition and galloping over unperceived obstacles of a quadruped robot with cpg modulated by vestibular feedback. *Robotics Auton. Syst.* **111**, 1–19 (2019).
31. Aoi, S., Yamashita, T. & Tsuchiya, K. Hysteresis in the gait transition of a quadruped investigated using simple body mechanical and oscillator network models. *Phys. Rev. E* **83**, 061909 (2011).
32. Aoi, S. *et al.* A stability-based mechanism for hysteresis in the walk–trot transition in quadruped locomotion. *J. The Royal Soc. Interface* **10**, 20120908 (2013).
33. Diedrich, F. J. & Warren Jr, W. H. Why change gaits? dynamics of the walk-run transition. *J. Exp. Psychol. Hum. Percept. Perform.* **21**, 183 (1995).
34. Diedrich, F. & Warren, W. Dynamics of human gait transitions. *Timing behavior: Neural, psychological, computational perspectives* 323–343 (1998).
35. Fu, Z., Kumar, A., Malik, J. & Pathak, D. Minimizing energy consumption leads to the emergence of gaits in legged robots. In Faust, A., Hsu, D. & Neumann, G. (eds.) *Proceedings of the 5th Conference on Robot Learning*, vol. 164 of *Proceedings of Machine Learning Research*, 928–937 (PMLR, 2022).
36. Shao, Y. *et al.* Learning free gait transition for quadruped robots via phase-guided controller. *IEEE Robotics Autom. Lett.* **7**, 1230–1237, DOI: [10.1109/LRA.2021.3136645](https://doi.org/10.1109/LRA.2021.3136645) (2022).
37. Bellegarda, G., Chen, Y., Liu, Z. & Nguyen, Q. Robust high-speed running for quadruped robots via deep reinforcement learning. In *2022 IEEE/RSJ International Conference on Intelligent Robots and Systems (IROS)*, 10364–10370, DOI: [10.1109/IROS47612.2022.9982132](https://doi.org/10.1109/IROS47612.2022.9982132) (2022).
38. Caluwaerts, K. *et al.* Barkour: Benchmarking animal-level agility with quadruped robots. *arXiv preprint arXiv:2305.14654* (2023).
39. Fuchioka, Y., Xie, Z. & van de Panne, M. Opt-mimic: Imitation of optimized trajectories for dynamic quadruped behaviors. *arXiv preprint arXiv:2210.01247* (2022).

40. Li, C. *et al.* Learning agile skills via adversarial imitation of rough partial demonstrations. In *Conference on Robot Learning*, 342–352 (PMLR, 2023).
41. Smith, L. *et al.* Learning and adapting agile locomotion skills by transferring experience. *arXiv preprint arXiv:2304.09834* (2023).
42. Kang, D., Cheng, J., Zamora, M., Zargarbashi, F. & Coros, S. RL+ model-based control: Using on-demand optimal control to learn versatile legged locomotion. *arXiv preprint arXiv:2305.17842* (2023).
43. Yang, Y., Zhang, T., Coumans, E., Tan, J. & Boots, B. Fast and efficient locomotion via learned gait transitions. In *Conference on Robot Learning*, 773–783 (PMLR, 2022).
44. Wieber, P.-B. Viability and predictive control for safe locomotion. In *2008 IEEE/RSJ International Conference on Intelligent Robots and Systems*, 1103–1108 (IEEE, 2008).
45. Wieber, P.-B. On the stability of walking systems. In *Proceedings of the international workshop on humanoid and human friendly robotics* (2002).
46. Shafiee, M., Bellegarda, G. & Ijspeert, A. Puppeteer and marionette: Learning anticipatory quadrupedal locomotion based on interactions of a central pattern generator and supraspinal drive. *2023 IEEE Int. Conf. on Robotics Autom.* (2023).
47. McVea, D. & Pearson, K. Contextual learning and obstacle memory in the walking cat. *Integr. Comp. Biol.* **47**, 457–464 (2007).
48. Kalakrishnan, M., Buchli, J., Pastor, P., Mistry, M. & Schaal, S. Learning, planning, and control for quadruped locomotion over challenging terrain. *The Int. J. Robotics Res.* **30**, 236–258 (2011).
49. Magana, O. A. V. *et al.* Fast and continuous foothold adaptation for dynamic locomotion through cnns. *IEEE Robotics Autom. Lett.* **4**, 2140–2147 (2019).
50. Yu, W. *et al.* Visual-locomotion: Learning to walk on complex terrains with vision. In *5th Annual Conference on Robot Learning* (2021).
51. Lee, K.-H. *et al.* Pi-ars: Accelerating evolution-learned visual-locomotion with predictive information representations. In *2022 IEEE/RSJ International Conference on Intelligent Robots and Systems (IROS)*, 1447–1454 (IEEE, 2022).
52. Agarwal, A., Kumar, A., Malik, J. & Pathak, D. Legged locomotion in challenging terrains using egocentric vision. *arXiv preprint arXiv:2211.07638* (2022).
53. Xie, Z., Da, X., Babich, B., Garg, A. & de Panne, M. v. Glide: Generalizable quadrupedal locomotion in diverse environments with a centroidal model. In *Algorithmic Foundations of Robotics XV: Proceedings of the Fifteenth Workshop on the Algorithmic Foundations of Robotics*, 523–539 (Springer, 2022).
54. Agrawal, A., Chen, S., Rai, A. & Sreenath, K. Vision-aided dynamic quadrupedal locomotion on discrete terrain using motion libraries. In *2022 International Conference on Robotics and Automation (ICRA)*, 4708–4714 (IEEE, 2022).
55. Margolis, G. B. *et al.* Learning to jump from pixels. In *Proceedings of the 5th Conference on Robot Learning*, vol. 164 of *Proceedings of Machine Learning Research*, 1025–1034 (PMLR, 2022).
56. Rudin, N., Hoeller, D., Bjelonic, M. & Hutter, M. Advanced skills by learning locomotion and local navigation end-to-end. In *2022 IEEE/RSJ International Conference on Intelligent Robots and Systems (IROS)*, 2497–2503 (IEEE, 2022).
57. Yang, R., Yang, G. & Wang, X. Neural volumetric memory for visual locomotion control. In *Proceedings of the IEEE/CVF Conference on Computer Vision and Pattern Recognition*, 1430–1440 (2023).
58. Wickler, S., Hoyt, D., Cogger, E. & McGuire, R. The cost of transport in an extended trot. *Equine Vet. J.* **34**, 126–130 (2002).
59. Whishaw, I. Q., Sacrey, L.-A. R. & Gorny, B. Hind limb stepping over obstacles in the horse guided by place-object memory. *Behav. brain research* **198**, 372–379 (2009).
60. Cox, S., Ekstrom, L. & Gillis, G. The influence of visual, vestibular, and hindlimb proprioceptive ablations on landing preparation in cane toads. *Integr. Comp. Biol.* **58**, 894–905 (2018).

61. Griffin, T. M., Kram, R., Wickler, S. J. & Hoyt, D. F. Biomechanical and energetic determinants of the walk–trot transition in horses. *J. Exp. Biol.* **207**, 4215–4223 (2004).
62. Danner, S. M., Shevtsova, N. A., Frigon, A. & Rybak, I. A. Computational modeling of spinal circuits controlling limb coordination and gaits in quadrupeds. *Elife* **6**, e31050 (2017).
63. Heim, S. & Spröwitz, A. Beyond basins of attraction: Quantifying robustness of natural dynamics. *IEEE Transactions on Robotics* **35**, 939–952 (2019).
64. Patil, N. S., Dingwell, J. B. & Cusumano, J. P. Viability, task switching, and fall avoidance of the simplest dynamic walker. *Sci. reports* **12**, 8993 (2022).
65. Wieber, P.-B., Tedrake, R. & Kuindersma, S. Modeling and control of legged robots. In *Springer handbook of robotics*, 1203–1234 (Springer, 2016).
66. Hof, A., Gazendam, M. & Sinke, W. The condition for dynamic stability. *J. biomechanics* **38**, 1–8 (2005).
67. Shafiee, M., Romualdi, G., Dafarra, S., Chavez, F. J. A. & Pucci, D. Online dcm trajectory generation for push recovery of torque-controlled humanoid robots. In *2019 IEEE-RAS 19th International Conference on Humanoid Robots (Humanoids)*, 671–678 (IEEE, 2019).
68. Yeganegi, M. H., Khadiv, M., Del Prete, A., Moosavian, S. A. A. & Righetti, L. Robust walking based on mpc with viability guarantees. *IEEE Transactions on Robotics* **38**, 2389–2404 (2021).
69. Toebes, M. J., Hoozemans, M. J., Furrer, R., Dekker, J. & van Dieën, J. H. Local dynamic stability and variability of gait are associated with fall history in elderly subjects. *Gait & posture* **36**, 527–531 (2012).
70. Rohatgi, A. Webplotdigitizer: Version 4.6 (2022).
71. Rybak, I. A., Shevtsova, N. A., Lafreniere-Roula, M. & McCrea, D. A. Modelling spinal circuitry involved in locomotor pattern generation: insights from deletions during fictive locomotion. *The J. physiology* **577**, 617–639 (2006).
72. Bellegarda, G. & Ijspeert, A. CPG-RL: Learning central pattern generators for quadruped locomotion. *IEEE Robotics Autom. Lett.* **7**, 12547–12554 (2022).
73. Fukuhara, A., Owaki, D., Kano, T., Kobayashi, R. & Ishiguro, A. Spontaneous gait transition to high-speed galloping by reconciliation between body support and propulsion. *Adv. robotics* **32**, 794–808 (2018).
74. Schulman, J., Moritz, P., Levine, S., Jordan, M. I. & Abbeel, P. High-dimensional continuous control using generalized advantage estimation. *CoRR* **abs/1506.02438** (2015).
75. Coumans, E. & Bai, Y. Pybullet, a python module for physics simulation for games, robotics and machine learning. <http://pybullet.org> (2016–2019).
76. Rudin, N., Hoeller, D., Reist, P. & Hutter, M. Learning to walk in minutes using massively parallel deep reinforcement learning. In Faust, A., Hsu, D. & Neumann, G. (eds.) *Proceedings of the 5th Conference on Robot Learning*, vol. 164 of *Proceedings of Machine Learning Research*, 91–100 (PMLR, 2022).
77. Makoviychuk, V. *et al.* Isaac gym: High performance gpu-based physics simulation for robot learning. *arXiv preprint arXiv:2108.10470* (2021).
78. Unitree Robotics. A1 (2021).
79. Herr, H. & Popovic, M. Angular momentum in human walking. *J. experimental biology* **211**, 467–481 (2008).

Acknowledgements

We would like to thank Alessandro Crespi for assisting with hardware setup. This research is supported by the Swiss National Science Foundation (SNSF) as part of project No.197237.

Author contributions statement

M.Sh.: conceptualisation, formal analysis, software, simulation, hardware experiment, investigation, writing original draft, visualisation; G.B.: conceptualisation, formal analysis, software, simulation, writing, review & editing; A.I.: conceptualisation, formal analysis, review & editing, supervision, funding acquisition;

Competing interests

The authors declare no competing interests.

Description of Additional Supplementary Files

DeepTransition: Viability Leads to the Emergence of Gait Transitions in Learning Anticipatory Quadrupedal Locomotion Skills

Supplementary Movie 1.

Description: Hardware experiments of gait transition (Figure 7) [\[Link\]](#)

Supplementary Movie 2.

Description: Gap crossing in Pybullet (Figure 3) [\[Link\]](#)

Supplementary Movie 3.

Description: Gap crossing in Isaac Gym, reward function analysis (Figure 4) [\[Link\]](#)

Supplementary Movie 4.

Description: Gap crossing in PyBullet, observation space and gait coupling analysis (Figure 5) [\[Link\]](#)

Supplementary Movie 5.

Description: Gap crossing in Isaac Gym, small contact surface between gaps (Figure 8-a) [\[Link\]](#)

Supplementary Movie 6.

Description: Locomotion across small stepping stones (Figure 8-b) [\[Link\]](#)

Supplementary Movie 7.

Description: Locomotion across a net-like terrain (Figure 8-c) [\[Link\]](#)

Supplementary Movie 8.

Description: Locomotion across mixed stepping stones (Figure 8-d) [\[Link\]](#)

Supplementary Data 1:

Description: Source data for Figures 2, 4 and 5. [\[Link\]](#)

Supplementary Material

DeepTransition: Viability Leads to the Emergence of Gait Transitions in Learning Anticipatory Quadrupedal Locomotion Skills

This file contains the following supplementary information:

Supplementary Note S.1.

Description: Reinforcement learning training details and parameters.

Supplementary Note S.2.

Description: Reward function terms for flat terrain and gap crossing scenarios.

Supplementary Note S.3.

Description: DCM and viability concept.

Supplementary Note S.4.

Description: Phase coupling matrices for different gaits.

Supplementary Note S.5.

Description: Supraspinal signals.

S.1 Training details

We use PyBullet⁷⁵ and Isaac Gym⁷⁷ as our physics engines for training and simulation purposes, and the Unitree A1 and Go1 quadruped robots⁷⁸. Table S.1.1 summarizes the training schemes for the flat terrain and gap crossing scenarios. To train the policies, we use Proximal Policy Optimization (PPO)⁷⁴, a state-of-the-art on-policy algorithm for solving the MDP, and Table S.1.2 shows the PPO hyperparameters and neural network architecture for PyBullet simulation. The control frequency of the policy is 100 Hz, and the torques computed from the desired joint positions are updated at 1 kHz. The equations for each of the oscillators (Eq. (1) and (2) in the main text) are thus also integrated at 1 kHz. The joint PD controller gains are $K_p = 100, K_d = 2$. All policies in PyBullet and Isaac Gym are trained for 3.5×10^7 and 36.4×10^7 samples respectively.

Table S.1.1. Summary of experimental scenarios.

Options \ Exp Name	Flat Terrain	Gap Crossing
Simulator	PyBullet	PyBullet/Isaac Gym
Animal Data	✓	×
Investigated Criteria	Viability/Energy	Viability/Peak Force/Energy
Neural gait coupling	Walk/Trot	Without Coupling
Blind Observation space	✓	✓
$\mathbf{a}_{off} = [\mathbf{x}_{off}] \in \mathbb{R}^4$ in Action space	×	✓
$\mathbf{a}_{osc} = [\boldsymbol{\mu}, \boldsymbol{\omega}] \in \mathbb{R}^8$ in Action space	✓	✓
Exteroceptive Observation Space	×	LiDAR/Explicit Features/Height Map
Reward for Minimizing Energy	✓	✓
Reward for Viability	✓	✓
Reward for Peak Contact Force	×	✓
Reward for Velocity Tracking	✓	×
Reward for Penalizing Body Orientation	✓	✓

Table S.1.2. PPO Hyperparameters and neural network architecture used with PyBullet.

Parameter	Value	Parameter	Value
Batch size	4096	GAE discount factor	0.95
Mini-batch size	128	Desired KL-divergence kl^*	0.01
Number of epochs	10	Learning rate α	1e-4
Clip range	0.2	NN Hidden Layers	[256,256]
Entropy coefficient	0.01	Activation	tanh
Discount Factor	0.99	Framework	Torch

Table S.1.3. PPO Hyperparameters and neural network architecture used with Isaac Gym.

Parameter	Value	Parameter	Value
Batch size	98304 (4096x24)	GAE discount factor	0.95
Mini-batch size	24576 (4096x6)	Desired KL-divergence kl^*	0.01
Number of epochs	5	Learning rate α	adaptive
Clip range	0.2	NN Hidden Layers	[512, 256, 128]
Entropy coefficient	0.01	Activation	elu
Discount factor	0.99	Framework	Torch

Table S.1.3 shows the PPO hyperparameters and neural network architecture used with Isaac Gym. Figure S.1.1 illustrates the height-map as exteroceptive information that is used for training policies in Isaac Gym.

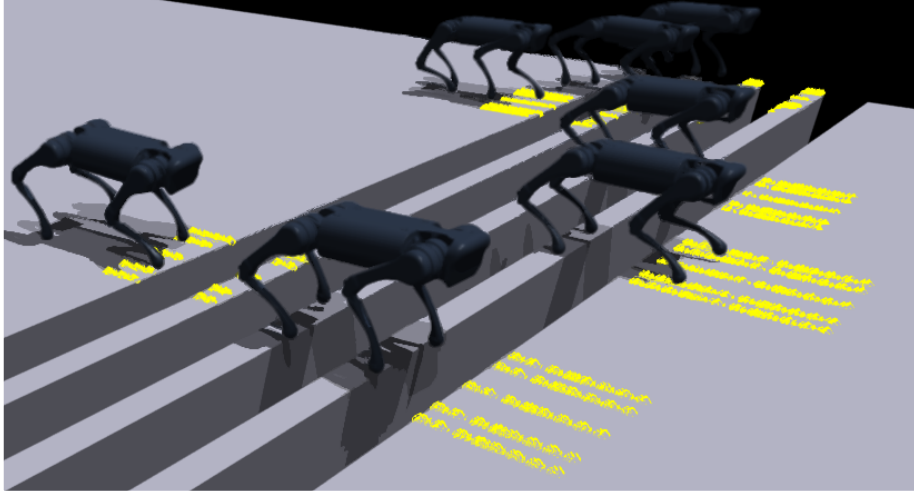


Figure S.1.1. Height-Map data around the robot in Isaac Gym.

S.2 Reward Function Terms

Reward Function for Blind Locomotion on Flat Terrain: We design our reward function to promote viable states and fall prevention, tracking a desired base velocity, and minimizing energy expenditure as follows:

$$r_1 = \alpha_{1,flat} \cdot \min(f_x, d_{max}) + \alpha_{2,flat} \cdot \exp\left(-\frac{\|\mathbf{v}_{des} - \mathbf{v}_{real}\|^2}{0.25}\right) + \alpha_{3,flat} \cdot |\boldsymbol{\tau} \cdot (\dot{\mathbf{q}}^t - \dot{\mathbf{q}}^{t-1})| + \alpha_{4,flat} \cdot \|\mathbf{o}_{base} - \mathbf{o}_{zero}\|$$

- *Forward progress (promoting viability):* In the first term, f_x corresponds to forward progress in the world (along the x-direction). This term promotes viability of the system, as continuous high forward progress indicates that the robot has not fallen. Additionally in r_2 below, forward progress in a gap crossing scenario indicates that the robot is able to traverse the gaps without falling. We limit this term to avoid exploiting simulator dynamics and achieving unrealistic speeds, where d_{max} is the maximum distance/reward the robot can receive for moving forward over the last control cycle ($\alpha_{1,flat} = 0.03$).
- *Velocity tracking reward:* In the second term, \mathbf{v}_{des} and \mathbf{v}_{real} correspond to desired and real (actual) locomotion velocity in the world x-direction. This term encourages the robot to follow the desired locomotion velocity. This term also promotes viability of the system, as tracking the steady state velocity indicates that the robot has not fallen ($\alpha_{2,flat} = 0.03$).
- *Power:* The fourth term penalizes power in order to find energy efficient gaits, where $\dot{\mathbf{q}}$ and $\boldsymbol{\tau}$ are vectors of all of the joint velocities and torques ($\alpha_{3,flat} = -0.00001$).
- *Base orientation penalty:* The third term penalizes body orientation deviations from the nominal base horizontal configuration ($\alpha_{4,flat} = -0.02$). Large roll and pitch angles increase the likelihood of falling, thus penalizing these occurrences helps to prevent the system from getting closer to the boundary of the viability kernel.

Reward Function for Gap Crossing: To analyze the effects of the different reward function terms, for gap crossing scenarios

Table S.2.1. Reward function term weights for flat terrain and gap-crossing scenarios.

Reward function term weights				
Terms	Flat Terrain	Gap Terrain		
Viability	$\alpha_{1,flat} = 0.03$	$\alpha_{1,gap,low} = 0.1$	$\alpha_{1,gap,medium} = 4.0$	$\alpha_{1,gap,high} = 8.0$
Velocity Tracking	$\alpha_{2,flat} = 0.03$	×		
Peak Contact Force	×	$\alpha_{2,gap,low} = -0.0001$	$\alpha_{2,gap,medium} = -0.001$	$\alpha_{2,gap,high} = -0.01$
Power	$\alpha_{3,flat} = -0.00001$	$\alpha_{3,gap,low} = -0.00001$	$\alpha_{3,gap,medium} = -0.0001$	$\alpha_{3,gap,high} = -0.001$
Base Orientation	$\alpha_{4,flat} = -0.02$	$\alpha_{4,gap} = -0.25$		

we consider the following reward function r_2 with varying low, medium, and high weights, summarized in Table S.2.1. The low and medium weights are selected to be approximately 1% and 50% of the high values, respectively.

$$r_2 = \alpha_{1,gap} \cdot \min(f_x, d_{max}) + \alpha_{2,gap} \cdot \sum_{i=1}^4 \max(0, F_{c,i} - F_{c,max}) + \alpha_{3,gap} \cdot |\boldsymbol{\tau} \cdot (\dot{\boldsymbol{q}}^t - \dot{\boldsymbol{q}}^{t-1})| + \alpha_{4,gap} \cdot \|\boldsymbol{o}_{base} - \boldsymbol{o}_{zero}\|$$

- *Forward progress (promoting viable states)*: Regarding forward progress, we assign 8.0, 4.0, and 0.1 as the high, medium, and low values, respectively, for the parameter $\alpha_{1,gap}$.
- *Peak contact force*: To penalize the peak contact reaction forces, we assign -0.01 , -0.001 , and -0.0001 as high, medium, and low weights, respectively, for the parameter $\alpha_{2,gap}$. The determination of the maximum contact force, denoted as $F_{c,max} = 180N$, was accomplished through monitoring the contact reaction force during locomotion on flat terrain at a speed of 1.2 m/s.
- *Power*: For penalizing power, we assign -0.001 , -0.0001 , and -0.00001 as the high, medium, and low weights, respectively, for the parameter $\alpha_{3,gap}$.
- *Base orientation penalty*: For penalizing the body orientation deviations, we use $\alpha_{4,gap} = -0.25$.

S.3 DCM offset and Viability

S.3.1 Linear Inverted Pendulum

The linear inverted pendulum model (LIPM) has been widely used for modeling the Center of Mass (CoM) dynamics for bipedal locomotion⁶⁶. Briefly, the LIPM assumes that the rate change of the centroidal angular momentum is zero, and the CoM height moves in a plane. These assumptions are acceptable for locomotion planning for humanoid and quadruped robots, as studies on human walking have shown that the centroidal angular momentum and change of height of the CoM of the human body during walking is very small⁷⁹. With these assumptions, the equations of motion of the LIPM can be derived as:

$$\ddot{r}_{CoM} = \omega^2(r_{CoM} - r_{CoP}) \quad (\text{S.3.1})$$

where r_{CoM} is the horizontal position of the CoM, $\omega_0 = \sqrt{\frac{g}{\Delta z}}$ is the natural frequency of the LIPM, and r_{CoP} is the horizontal position of the Center of Pressure (CoP) (Figure (S.3.1)-A). Here, Δz represents the CoM height, and g denotes the gravitational acceleration.

S.3.2 Divergent Component of Motion (DCM) Dynamics

In this section, we review the Divergent Component of Motion (DCM). The CoM dynamics can be decomposed into stable and unstable components. The DCM represents the unstable part, and is defined as:

$$\xi = r_{CoM} + \frac{\dot{r}_{CoM}}{\omega} \quad (\text{S.3.2})$$

By re-ordering Equation (S.3.2), the CoM dynamics are given by:

$$\dot{x} = \omega(\xi - x) \quad (\text{S.3.3})$$

Differentiating Equation (S.3.2) and substituting into Equation (S.3.3), the DCM dynamics can be expressed as:

$$\dot{\xi} = \omega(\xi - r_{CoP}) \quad (\text{S.3.4})$$

Figure S.3.1-A shows the relationship between the DCM dynamics and the CoP. By solving Equations (S.3.3) and (S.3.4) as an initial value problem, we have:

$$r_{CoM} = (r_{CoM,0} - \xi_0) \exp(-\omega t) + \xi_0 \quad (\text{S.3.5})$$

$$\xi = (\xi_0 - r_{CoP,0}) \exp(\omega t) + r_{CoP,0} \quad (\text{S.3.6})$$

The CoM has stable dynamics since the exponential term is negative. However, the DCM has unstable dynamics as the

exponential term is positive, which implies that the DCM position grows exponentially with time. A sufficient condition for stability of the CoM trajectory is that the DCM trajectory is stable. We define $b_\xi = \xi_0 - r_{CoP,0}$ as the DCM offset, which can directly amplify the rate of divergence of the DCM dynamics.

S.3.3 Viability

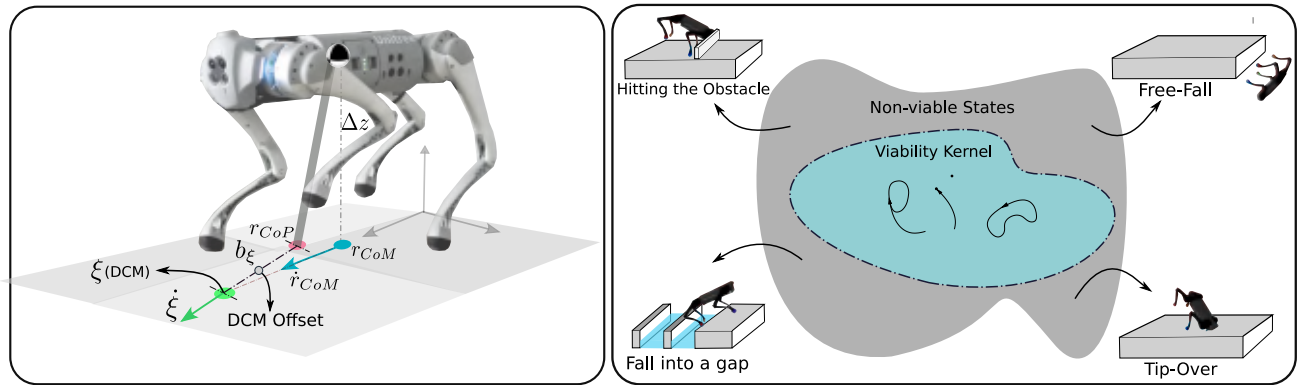


Figure S.3.1. A: Inverted Pendulum and DCM, B: Viability Kernel⁴⁴

The viability kernel encompasses all states from which the mobile system can avoid falling or colliding with obstacles through corrective control actions. Outside of this set, these outcomes are unavoidable (Figure S.3.1). It has been shown that for bipedal locomotion on flat terrain, and considering only foot swing phase, we can determine viable and nonviable locomotion states based on a critical DCM offset (b_ξ)⁶⁸. However, such a method to calculate the critical value of the DCM offset does not yet exist for quadrupeds due to the inclusion of multiple support phases at each step. Nevertheless, we can still use the DCM offset for quantifying the viability of quadruped robot, as the quadruped dynamics are described by the LIPM. In another words, by increasing the DCM offset, the system approaches nonviable falling states.

S.4 Phase coupling for different gaits

The coupling matrix Φ representing a walk, trot and bound gaits can be defined as:

$$\Phi_{gait} = \begin{bmatrix} 0 & -A & -B & -C \\ A & 0 & A-B & A-C \\ B & B-A & 0 & B-C \\ C & C-A & C-B & 0 \end{bmatrix} \quad (\text{S.4.1})$$

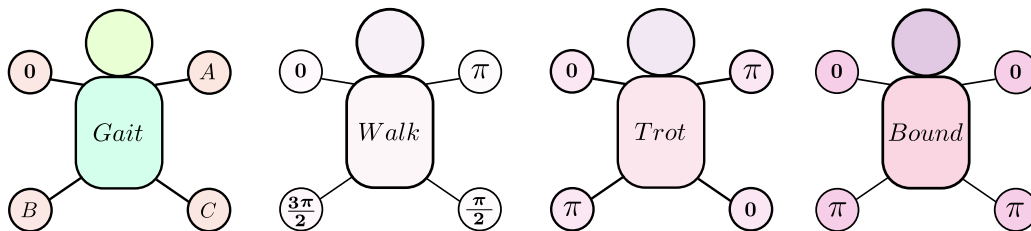


Figure S.4.1. Phase coupling for different gaits.

where the row/column order is Front Left (FL), Front Right (FR), Hind Left (HL), Hind Right (HR) and A , B and C are defined in Figure S.4.1.

S.5 Supraspinal Signals

Figure S.5.1 shows the supraspinal drive performing complex interlimb coordination by modulating each limb's frequency, amplitude, and foot position offset in order to successfully cross eight consecutive gaps. On average, the limb frequency increases to near the maximum for all legs before/after crossing each of the gaps (shadow bars). The amplitude for the front limbs distinctly increases while over the gap in order to take a larger step, which together with the offset terms are also important components for interlimb coordination. The offset terms go from positive hip x offsets to negative hip x offsets to help cross the gaps for all limbs.

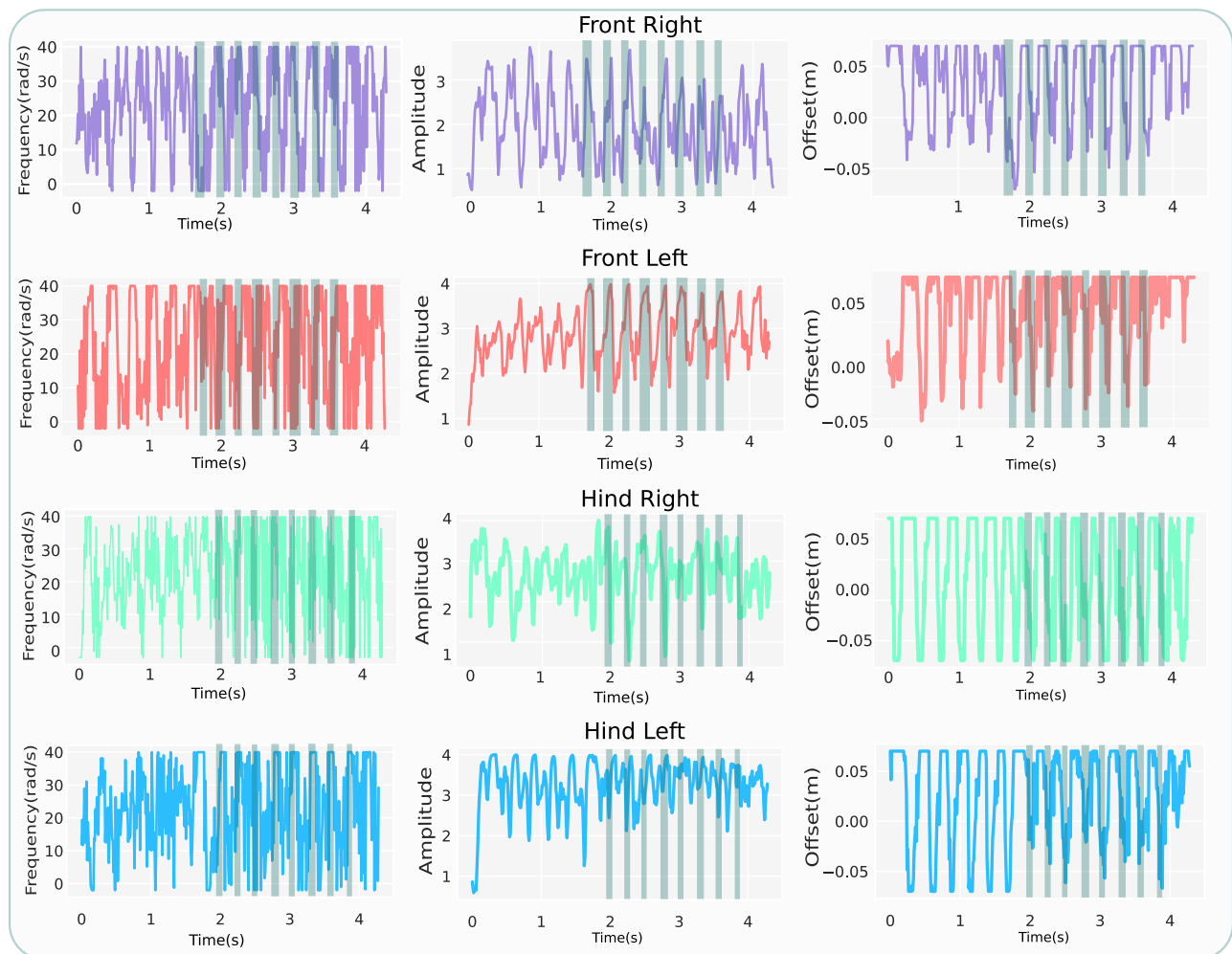


Figure S.5.1. CPG frequency, amplitude, and offset for the limbs. The shadow bars indicate when the foot is over a gap.